博士論文

Neuronal responses of primary motor cortex evoked by activation of dopamine neurons in the ventral midbrain : an optical imaging study

（中脳ドーパミンニューロン賦活化により

一次運動野皮質に誘発される神経活動の光学的解析）

平成２６年度

筑波大学大学院　人間総合科学研究科　感性認知脳科学専攻

九里　信夫

筑波大学

Table of contents

Abstract

Dopamine (DA) neurotransmission is involved in many behavioral functions, including reward-motivated learning, control of movement, and motor skill learning. Recently, some studies focused on the DA inputs to the primary motor cortex (M1) because of their contribution in motor recovery after brain damage. The M1 receives DA projections mainly from the ventral tegmental area (VTA) through the mesocortical DA pathway. However, M1 neuronal activity resulting from the VTA activation is still unknown. In the present study, I used voltage sensitive dye (VSD) imaging to reveal the spatiotemporal dynamics of M1 activity induced by single pulse stimulation of the VTA in anesthetized rats. VSD imaging showed that brief electrical stimulation of unilateral VTA elicited a short-latency excitatory-inhibitory sequence of neuronal activity in both sides of M1. VTA-evoked M1 response in contralateral M1 was not affected by pharmacological blockade of ipsilateral M1 activity, but it was completely abolished by corpus callosum transection. Although the VTA-evoked neuronal activity extended throughout the entire M1, I found the most prominent activity in the forelimb area. The M1 response was not induced after 6-hydroxydopamine lesion of the VTA. Furthermore, both excitatory and inhibitory activity was entirely extinguished by blocking glutamate receptors in the target M1. When intracortical microstimulation of M1 was paired with VTA stimulation, the

evoked forelimb muscle activity was facilitated or inhibited, depending on the interval between the two stimuli. These findings suggest that VTA neurons modulate the excitability of M1 neurons via glutamate signaling and, consequently, may control the last cortical stage of motor command processing.

Abbreviations

ACSF: artificial cerebrospinal fluid

CC: corpus callosum

CFA: caudal forelimb area

CNQX: 6-cyano-7-nitroquinoxaline-2,3-dione

CNS: central nervous system

CSD: current source density

DA: dopamine

DAB: 3,3'-diaminobenzidine

EMG: electromyogram

fMRI: functional magnetic resonance imaging

GABA: gamma aminobutyric acid

ICMS: intracortical microstimulation

ISI: inter stimulus interval

LFP: local field potential

LTP: long-term potentiation

M1: primary motor cortex

NAc: nucleus accumbens

PBS: phosphate buffered saline

PFC: prefrontal cortex

RFA: rostral forelimb area

ROI: region of interest

SNc: substantia nigra pars compacta

TH: tyrosine hydroxylase

VGLUT2: vesicular glutamate transporter 2

Vib: vibrissae motor area

VSD: voltage sensitive dye

VTA: ventral tegmental area

6-OHDA: 6-hydroxydopamine

Introduction

Dopamine system is involved in motor function

Animals including human being have an ability to move their own body in a purposeful manner. The planning, executing and controlling the immense repertories of voluntary movements are achieved by the appropriate motor commands from the central nervous system (CNS), in which the motor centers of the brain and spinal cord generate neuronal signals for coordinated and purposeful movements. For this reason, lesion of the motor system in the CNS causes variety of motor symptoms, such as the weakness and spasticity seen with stroke and spinal cord injury, and slowness of movement initiation and termination typical of Parkinson's disease.

Recently, using a spinal cord injury model in monkeys, a brain imaging study demonstrated that recovery of precise finger movement was accompanied by increased activity not only in motor related brain areas, particularly in the primary motor cortex (M1), but also in motivation related brain areas, such as nucleus accumbens (NAc) and ventral tegmental area (VTA) (Nishimura et al., 2011). Because motivation system is considered to relate to the dopamine (DA) neurotransmission (Wise, 2004), the functional connectivity between the DA and the M1 has attracted considerable attention to improve motor recovery after CNS damage (Luft and Schwarz, 2009; Ruscher et al., 2012;

Nishimura et al., 2011; Lindenbach and Bishop, 2013).

The DA system is involved in many brain functions, including reward, expectation, motivation, emotion, control of movement, and motor skill learning (Shultz, 2002, 2007; Wise, 2004; Luft and Schwarz, 2009; Redgrave et al., 2010). Involvement of the DA system in motor functions is evident because pathological changes of DA system cause motor abnormalities. A well-known example is the Parkinson's disease, which affects DA neurons in the substantia nigra pars compacta (SNc) that project predominantly to the dorsal striatum (Matsuda et al., 2009; Redgrave et al., 2010). The loss of DA in Parkinson's disease is considered to cause motor symptoms, such as tremor, rigid muscle and slowed movement, because these impairments respond to DA replacement therapies (Smith et al., 2012). Although how DA signal modulates function of the dorsal striatum is still controversial (Shen et al., 2008; Redgrave et al., 2010), elucidation of the functional relationship between the DA system and the motor system advances clinical treatment of patients with motor deficit (Smith et al., 2012). However, at present, functional connectivity between the M1 and the DA system is not well understood.

Primary motor cortex is crucial for motor execution and learning

The M1 is an origin of the descending neuronal pathways that transmit motor commands

to the spinal neurons directly through the corticospinal tract and indirectly via the brain stem nucleus (Lawrence and Kuypers, 1968; Esposito et al., 2014). When conscious control is required, the descending motor signals control precise limb movements (Lawrence and Kuypers, 1968; Esposito et al., 2014), and stereotyped rhythmic movements, such as locomotion (Drew et al., 2008). The M1 contains the most detailed motor map in contrast to the higher-order motor areas, and has been considered essential in the execution of movements because neuronal activity of the M1 closely related to the muscle activity and joint movement rather than the planning of movement (Kakei et al., 1999; Cisek et al., 2003).

As well as movement execution, accumulative evidence suggests that the M1 is a crucial brain region for motor skill learning. Motor skills are acquired by trial-and-error learning, and is implicitly stored in the brain as motor memory (Squire, 2004). Over the past two decades, neuroscientists have begun to use brain imaging techniques, such as functional magnetic resonance imaging (fMRI), to investigate the changes in brain activity during motor learning. Previous human fMRI studies revealed that the learning of sequential finger movements increased M1 activity, which followed more rapid changes of activity in cerebellum, dorsal striatum and other motor related cortex (Karni et al., 1995, 1998; Ungerleider et al., 2002). These results indicate that the activated-brain

areas are sequentially changed with advance of the learning processes. Because both cerebellum and striatum form two distinct neuronal loops between the motor cortex, subcortical circuits is thought to contribute particularly in early phase of motor skill learning (Middleton and Strick, 2000; Ungerleider et al., 2002). Furthermore, increase of M1 activity in the later phase of motor learning can reflect involvement of M1 in maintenance of motor memory (Karny et al., 1995, 1998; Ungerleider et al., 2002; von-Kraus et al., 2010).

Practice dependent modulation of M1 activity was accompanied with plastic changes in the M1 neuronal network. In animal experiments using reaching task, in which animals reach and grasp small food pellet through a small slit by precise hand movement, the motor representation of the hand extended with progress of task training (Nudo et al., 1996, Kleim et al., 1998, 2004). In addition to the reorganization of motor representations, morphological analysis revealed that the dendritic arborization and synaptic remodeling occurred in the M1 during motor skill training (Greenough et al., 1985; Kleim et al., 2004; Harms et al., 2008; Xu et al., 2009). Recent studies using *in vivo* calcium imaging showed that the task-specific activity patterns were generated in the M1 neurons during motor skill training (Huber et al., 2012; Peters et al., 2014; Masamizu et al., 2014).

A potent cellular mechanism in practice dependent modulation is long-term

potentiation (LTP), which is induced in M1 by motor skill training (Rioult-Pedotti et al., 1998, 2000). Using slice preparation of rat M1, Molina-Luna et al. (2009) showed that the LTP induction in layer 2/3 neurons were prevented by D1 and D2 like DA receptor antagonists. They also performed *in vivo* experiments and found that focal application of DA receptor antagonists into the M1 impaired motor skill acquisition without any effect in motor execution (Molina-Luna et al., 2009). The following study by von-Kraus et al. (2010) confirmed whether motor skills are memorized in the M1 through the LTP by using the zeta inhibitory peptide, the drug that prevents LTP maintenance. They found that previously acquired skilled-movement is completely disappeared by blocking the LTP maintenance in the M1 (von-Kraus et al., 2010). Therefore, motor memory is thought to be acquired and maintained by the LTP in the M1.

Ventral tegmental area is the major source of DA projection to the M1

The ascending DA projections originate from the mesencephalic DA neurons located in cytoarchitectonically defined two ventral midbrain regions: the SNc and the VTA (Fig. 2). Hosp et al. (2011) injected retrograde tracer into the forelimb motor area of the rat M1, and found that the VTA was the major source of DA projection to the M1 although SNc also provided a small DA projection. Because not only ipsilateral but also contralateral

VTA/SNc projects to M1 (Hosp et al., 2011), the unilateral M1 is thought to receive DA input from bilateral midbrain. VTA is composed of heterogeneous cell populations including DA neurons (~65%), gamma-aminobutyric acid (GABA) neurons (~35%), and glutamate neurons (2-3%), although relative amount of the VTA-glutamate neurons is still debated (Kawano et al., 2006; Nair-Roberts et al., 2008; Yamaguchi et al., 2011). The DA neurons in the VTA project wide range of cortical and subcortical brain areas such as the NAc, olfactory tubercle, septum, amygdala, and hippocampus (Swanson, 1982; Ikemoto, 2007). As well as DA neurons, glutamate and GABA neurons also project to several brain areas including the prefrontal cortex (PFC), NAc, ventral pallidum and lateral habenula (Carr and Sesack., 2000; Hnasko et al., 2012; Taylor et al., 2014). Both DA and non-DA VTA neurons project to the M1, but cell types of the non-DA neurons are remain uncertain (Hosp et al., 2011).

Since VTA neurons project to the cortex, the stimulation or chemical lesion of the VTA influences cortical remodeling. When electrical stimulation was applied to the VTA together with pure-tone stimulation, tonotopic representations in auditory cortex was extended selectively to that sound stimulus, but this cortical remodeling was suppressed by DA receptor antagonists (Bao et al., 2001). Meanwhile, pharmacological elimination of VTA-DA neurons impaired motor skill learning, but this impairment was partially

recovered by administration of levodopa (precursor of DA) into the M1 (Hosp et al., 2011).

Cortical DA terminals innervate throughout the cortical layers with regional and laminar specific manners. For example, in the rodent, all cortical layers in the PFC receive dense DA innervation with the highest density in layers 5-6, whereas M1 receives sparse DA innervation with a somewhat denser distribution in the layer 6. Existence of DA innervation in the rodent M1 is firstly reported by Berger and his colleagues (Berger et al., 1985, 1991; Descarries et al., 1987). They identified small number of DA fibers in layers 1-3 of M1 (Berger et al., 1985), and relatively large amount of DA-containing synaptic and non-synaptic (varicose-like) terminals in layer 6 (Descarries et al., 1987) (Fig. 1A). The synaptic and non-synaptic (varicose-like) terminals are hypothesized to be used in normal synaptic transmission and volume transmission, respectively (Descarries et al., 2008): the former type of neurotransmission is point-to-point communication between synapses, while the latter one is diffusion of neurotransmitter into the extracellular space to modulate neighboring neural activity (Fig. 1B).

DA neurons co-release DA and glutamate

It is well known that the DA neurons in VTA change their firing rate immediately after reward, reward-predicting stimuli, salient non-reward stimuli and novel or aversive

events (Horvitz, 2000; Schultz, 2002; Matsumoto and Hikosaka, 2009; Bromberg-Martin et al., 2010). Because firing activity sharply responds to the above events, DA neurons have been thought to encode temporally precise information, and these signals potentially influence neuronal activity in the target brain areas. However, DA neurotransmission is unsuitable for delivering such a temporally precise signal because increase of extracellular DA concentration is delayed from the DA neuron activation, and sustained over a few seconds (Garris and Wightman, 1994; Lavin et al., 2005). Therefore, some studies have proposed that DA neurons release glutamate from their terminals as co-transmitter for well-timed signal transmission (Lapish et al., 2007; Descarries et al., 2008).

The possibility of corelease of DA and glutamate from DA terminals has been suggested by the anatomical observations showing the vesicular glutamate transporter 2 (VGLUT2) at the axon terminals in the cultured DA neurons (Dal Bo et al., 2004), and the VGLUT2 mRNA in the somata of DA neurons (Kawano et al., 2006; Yamaguchi et al., 2011). Since VGLUT2 expression is higher in synaptic DA terminals than varicose-like DA terminal (Sulzer et al., 1998), a current hypothesis is that the synaptic terminals and varicose-like terminal are specialized to release glutamate and DA, respectively (Sulzer et al., 1998; Trudeau et al., 2004; Descarries et al., 2008). Physiological studies also provided evidence for glutamate signaling by DA neurons. Stuber et al. (2010)

activated the VGLUT2 expressing DA terminals in the NAc by using optogenetic methods, and found that optically-evoked excitatory post synaptic current in the NAc was blocked by glutamate receptor antagonist (Stuber et al., 2010). Similar result was obtained in the conditional knockout mice, which lack VGLUT2 expression in the DA neurons (Hnasko et al., 2012). Meanwhile, PFC receives projection from the VGLUT2 expressing DA neurons located in the VTA (Yamaguchi et al., 2011; Gorelova et al., 2012). Previous electrophysiological and optical imaging studies in the PFC revealed that electrical and pharmacological stimulation of the VTA elicited short-latency excitatory neuronal activity, which was abolished after the pharmacological lesion of the VTA-DA neurons and administration of a glutamate antagonist (Mercuri et al., 1985; Lavin et al., 2005, Watanabe et al., 2009). These studies suggest that VTA-DA neurons transmit glutamate signal to the PFC, but it is unknown whether similar fast signals are transmitted to the M1.

Problems

Previous studies suggest that ascending DA projections from the VTA to M1 contribute to motor skill learning (Hosp et al., 2011). If this is the case, activity of VTA-DA neurons in the particular situation during motor skill training (e.g. when unexpected success is

caused by some chance) should influence the M1 activity. A temporally precise signal transmission seems useful to reinforce the appropriate movement patterns and suppress inappropriate ones during motor skill training, but temporal discrepancy has been reported between DA neuron firing and cortical DA neurotransmission (Garris and Wightman, 1994; Lavin et al., 2005). Because VTA-DA neurons are considered to use glutamate for fast signal transmission (Descarries et al., 2008; Stuber et al., 2010), it is appropriate to hypothesize that the M1 receives glutamate signals through the mesocortical DA pathway. However, no reports have been described the short-latency glutamate neurotransmission in the M1 after VTA activation.

Another issue to be addressed is the projection from VTA to contralateral M1 hemisphere. Anatomical evidence indicates that VTA-DA neurons project bilaterally to the M1 (Hosp et al., 2011). Previous research has revealed that unilateral VTA lesioning enhance contralateral VTA activity, suggesting bilateral VTAs compensate each other (Majkutewicz et al., 2010). However, it is unknown whether VTA modulate contralateral M1 activity.

Objective and outline of this study

Based on the previous studies showing that the activation of VTA-DA neurons generates

fast glutamate signal in the PFC (Lavin et al., 2005), I hypothesized that the M1 received glutamate signal through the VTA-M1 DA pathway. In the present study, neuronal activity of the M1 in response to electrical stimulation of the VTA was characterized in anesthetized rat by *in vivo* voltage-sensitive dye (VSD) imaging. Contributions of DA neurons and glutamate neurotransmission to VTA-evoked M1 response were examined by using VTA-lesioned animals, and by performing the pharmacological blockade of glutamate receptors in the target M1, respectively. Furthermore, I examined contralateral M1 activity after the unilateral VTA activation. Finally, I explored modulatory effect of the VTA-evoked M1 response at the level of forelimb muscle activity by using electromyogram (EMG) with paired stimulation of the VTA and the M1.

In vivo *voltage sensitive dye imaging*

In the present study, *in vivo* VSD imaging was used as the main technique to record M1 activity. I mention the principles of VSD imaging in the following paragraph.

The neuronal activity is accompanied by the change of membrane potential; which is increased (depolarization) after excitatory synaptic inputs and action potential, while decreased (hyperpolarization) by inhibitory synaptic inputs. In VSD imaging, the preparations are stained by VSD and the fluctuation of membrane potential is measured

by converting it into the fluctuation of fluorescence signal from VSD. The dye molecules that are combined to the cell membrane during staining period emit fluorescence signal by irradiation of the excitation light (Fig. 3A). The intensity of fluorescence signal changes depending on the membrane potential. For example, fluorescence signal with VSD RH-795, which is used in the present study, increases when membrane potential shifts toward hyperpolarization and decreases when membrane potential shifts toward depolarization (Fig. 3B). Because electro-optical conversion occurs on the order of microseconds and intensity of fluorescence linearly correlated with membrane potential, high temporal resolution monitoring of fluorescence signal enables us to reveal the real-time change of membrane potential (Grinvald and Hildesheim, 2004).

In *in vivo* VSD imaging, fluorescence signal originates from the various neuronal and glial components including the dendrites, axons and somata. However, it is considered that the main source of optical signalis post synaptic potentials in the neuronal dendrites (Petersen et al., 2003). In my experiments, I also have the same opinion in regards to this point. Petersen et al. (2003) recorded whisker-evoked barrel cortex activity in the rat simultaneously by intracellular recording and VSD imaging. They found that the fluctuation of VSD signal well-correlated with the synaptic potential rather than spiking activity of neurons (Petersen et al., 2003). The fluorescence signal originates

predominantly (>95%) from membrane area in the layer 2/3 of the cortex, which including somata and dendrites of layer 2/3 neurons and dendrites of deeper layer neurons that extend into the layer 2/3 (Petersen et al., 2003; Takashima et al., 1999). This laminar restriction of VSD signal is caused from the limitation of the depth penetration of the dye molecules and the effect of light scattering by brain tissues. Although upper cortical layers include neuronal dendrite and somata, dendrites have far wider membrane areas than the neuronal somata (Grinvald and Hildesheim, 2004). Thus, majority of fluorescence signal is thought to arise from neuronal dendrites in the layers 1-3 of the cortex. Taken together, *in vivo* VSD signal does not imply occurrence of action potential at that site, rather it mainly reports the summation of dendritic activity in upper cortical layers.

Materials and Methods

Animals and surgical procedures

All experimental protocols were reviewed and approved by the Committee on Animal Care and Use and by the Ethical Committee of the National Institute of Advanced Industrial Science and Technology (AIST). Adult male Wistar rats (250–350 g) were used in all experiments. Animals were housed in standard cages under a 12 h light/dark cycle with food and water *ad libitum*. After anesthesia with an intraperitoneal (i.p.) injection of ketamine (80 mg/kg) and xylazine (10 mg/kg), rats were positioned in a stereotaxic frame (Narishige, Tokyo, Japan). Supplemental injections of ketamine and xylazine (i.p.) were used to maintain a constant level of anesthesia, as indicated by respiration rate, heart rate, whisker movement, and foot withdrawal reflex. Craniotomy was performed over the M1 [antero-posterior (A/P), –2.0 to +4.0 mm; medio-lateral (M/L), +1.5 to +5.5 mm from the bregma], and the VTA [A/P, –6.0 ± 0.5 mm; M/L, +0.5 mm from the bregma] (Paxinos and Watson, 1998). The exposed dura were carefully removed after a dental acrylic chamber was built on the skull around the cranial window above the M1. When I performed VSD imaging in the bilateral motor cortex, the cranial window and dental acrylic chamber were constructed on each hemisphere. A concentric bipolar electrode (Bio Research Center, Aichi, Japan) was positioned in the VTA at a depth of 7.5 ± 0.5

mm from the brain surface. When electrical stimulation was applied to the bilateral VTA, two concentric bipolar electrodes were positioned in the bilateral VTA. In additional animals (n = 3), concentric bipolar electrode (Bio Research Center) was positioned in the SNc at the following coordinates [A/P, −6.0 ± 0.5 mm; M/L, +1.0 to +3.0 mm from the bregma] (Paxinos and Watson, 1998). At the end of the experiments, a small electrolytic lesion was made by passing direct current (100 μA for 5 sec) to histologically confirm the stimulus site by Nissl staining.

In vivo *VSD imaging*

Thirty-two intact animals were used for *in vivo* VSD imaging (20 for unilateral and 12 for bilateral imaging). For *in vivo* VSD imaging, exposed motor cortex was stained for 1 h by VSD RH-795 (Life Technologies, Carlsbad, CA, USA) dissolved at 0.8 mg/mL in artificial cerebrospinal fluid (ACSF) containing the following (in mM): 125 NaCl, 5 KCl, 2 $CaCl_2$, 1.25 $MgSO_4$, 1.25 $NaHPO_4$, 22 $NaHCO_3$ and 10 glucose. The RH-795 has an excitation and emission maxima at 530 and 712 nm, respectively. Fluctuations in fluorescence from the dye decrease proportionally to the changes of membrane potentials, as described above. After dye incubation, unbound dye was thoroughly washed away and the dental acrylic chamber was sealed by a glass coverslip with ACSF. Fig. 4 shows a

block diagram of the experimental setup for VSD imaging with electrical stimulation of the VTA. Neuronal activity was recorded as fractional changes in fluorescence by a Micam01 system (Brainvision, Tokyo, Japan) using a tandem type epifluorescence microscope as previously reported (Takashima et al., 1999). The excitation light from tungsten-halogen lamp was filtered by band pass filter, and then reflected dawn onto the exposed brain surface by dichroic mirror (optical characteristics of filters and mirror are shown in Appendix). Emission from the cortex is projected to the CCD image sensor through the long pass filter. The optical signal was captured at 500 Hz with 88 × 60 pixels from approximately 4.5 × 3.0 mm of cortex. In each trial, single-pulse electrical stimulation was applied to the VTA (300 μs in duration and 150 μA in amplitude), and 16 consecutive trials with 16-s intervals were averaged to improve the signal-to-noise ratio. Optical signals were expressed relative to background fluorescence (ΔF/F). In this procedure, ΔF/F that exceeding the baseline noise was color-coded (Fig. 5). In the region of interest (ROI) analysis, ΔF/F was normalized to the maximum response value of each hemisphere. For statistical analyses of the optical responses, Kruskal-Wallis tests, and post hoc pairwise comparisons were performed using Bonferroni-corrected Mann-Whitney U-tests.

Local field potential recording

Local field potential (LFP) was recorded simultaneously with VSD imaging (Fig. 4 inset). A glass electrode filled with 0.5M NaCl was fixed at a micromanipulator and lowered near the M1 surface through the small slit of the glass coverslip. The voltage signal was filtered at 0.1-400 Hz and amplified (×100) with a Brownlee Precision Model 440 amplifier (Brownlee Precision, San Jose, CA, USA), digitized (sampling rate: 20 kHz; PCI-6023E, National Instruments, Austin, TX, USA), and stored on a personal computer running LabVIEW software (National Instruments).

Intracortical microstimulation

Motor representations was confirmed using an intracortical microstimulation (ICMS) technique (n = 3 animals). A flexible tungsten microelectrode (MicroProbes for Life Sciences, Gaithersburg, MD, USA) was positioned perpendicular to the cortical surface with a 500-μm grid. Electrical stimulation was delivered as 12 monophasic cathodal pulses (200 μs duration at 333 Hz, 5-50 μA). In each penetration, electrical stimulation was applied at a depth of 1,100-1,700 μm from the cortical surface, which corresponds to layers 5 and 6 of the M1. Evoked muscle contractions and movements were identified by visual inspection and palpation. The body part with the lowest movement threshold was

defined as the motor representations at that penetration, while the absence of detectable movement with 50 μA current intensity was defined as "no response." As for the forelimb areas in rodents, two motor areas have been identified: the caudal forelimb area (CFA) and the rostral forelimb area (RFA). The CFA and RFA were determined by surrounding motor representations, such as vibrissae, neck, jaw and no response areas.

When electrically evoked motor cortical activity was assessed (Fig. 11), the glass electrode filled with 0.5M NaCl was attached in a micromanipulator and inserted step wise (steps of 500 μm) from cortical surface into the CFA. In each step, motor cortical activity after single pulse stimulation (200 μs, 50-150 μA) was recorded by VSD imaging as described above.

Electromyogram recording

In the experiments of paired stimulation between the M1 and VTA (Figs. 19 and 20), muscle activity in upper limb were assessed by EMG recording (n = 6 animals). For stimulation of the M1, glass electrode filled with 0.5M NaCl was positioned within the M1 that showed the lowest movement threshold for elbow flexion, and delivered cathodal single pulse stimulation to generate the EMG response (200 μs, 50-150 μA). The evoked EMG activity was recorded from biceps brachii in contralateral forelimb with a concentric

bipolar electrode inserted near the center of the muscle fibers. Subsequently, the EMG was amplified (×100), filtered (0.3-10 kHz), digitized (sampling rate: 10 kHz; PCI-6023E, National Instruments), and stored on a personal computer running LabVIEW software (National Instruments). The EMG signal was rectified and averaged over 10 trials.

Current source density analysis

A silicon multiprobe electrode (Neuronexus Technologies Inc., Ann Arbor, MI, USA) with 16 × 100-μm linearly separated contact sites was used to record LFPs simultaneously throughout the motor cortical layers (n = 4 animals). The electrode was fixed to a micromanipulator and inserted perpendicular to the motor cortex at the following coordinates: A/P, 2.0 mm; M/L, 3.0 mm from the bregma. The electrode was inserted until upper most contact site was just visible. LFPs were acquired with 10 kHz after single pulse stimulation of the VTA (300 μs in duration and 150μA in current intensity). Voltage signals were amplified (×1,000) and filtered (bandwidth: 0.1–3 kHz) by a PBX preamplifier (Plexon Inc., Dallas, TX, USA), and then recorded through a Digidata 1320A interface (Molecular Devices, Sunnyvale, CA, USA). A set of LFPs was used for the current source density (CSD) analysis. CSD was computed as the second spatial derivative of the three adjacent sites using a standard method (Nicholson and Freeman,

1975; Mitzdorf, 1985). Contour plots of current sinks and sources were generated using the Origin software (OriginLab Corp., Northampton, MA, USA). The electrode tract and position were histologically verified by Nissl staining.

6-hydroxydopamine injection

DA neurons were destroyed by 6-hydroxydopamine (6-OHDA) injection directly into the unilateral VTA (n = 14 animals). One hour before injection, anesthetized animals were treated with desipramine hydrochloride (25 mg/kg, i.p.) to protect noradrenergic cells. The skull was exposed and a hole was drilled over the unilateral VTA to introduce a syringe for 6-OHDA (Sigma, St Louis, MO, USA) injection. A volume of 6 µL 6-OHDA (4 µg/µL in saline containing 0.1% ascorbic acid) was delivered at 0.25 µL/min into three separate injection sites using a motorized microinjector (IMS-10, Narishige). The needle was kept in place for an additional 5 min before it was slowly retracted. 6-OHDA-treated animals were used for experiments at least 4 weeks after the injection.

Pharmacological treatments

VTA stimulus-evoked responses were suppressed by microinjection of the $GABA_A$ receptor agonist muscimol into the motor cortex (n = 4 animals). Muscimol (Wako, Osaka,

Japan) was dissolved at a concentration of 1 μg/μL in saline and delivered into the cortex using a Hamilton syringe attached to a motorized microinjector (IMS-10, Narishige). A 0.1 μL-injection was performed in three to four penetrations at a depth of 1 mm from the cortical surface. Injection sites were determined according to the preceding VSD imaging results. The needle was kept in place for an additional 5 min at the end of the injection to prevent backflow of muscimol over the cortical surface.

In other experiments, I applied the AMPA/kainate glutamate receptor antagonist 6-cyano-7-nitroquinoxaline-2,3-dione (CNQX) (Sigma, 1 mM), the $GABA_A$ receptor antagonist bicuculline (Sigma, 100 μM), or the D1 receptor antagonist SCH 23390 HCl (Sigma, 100 μM) and the D2 antagonist S(±)-sulpiride (Sigma, 100 μM) onto the cortical surface (n = 3 animals each). Each pharmacological agent was dissolved in ACSF, and applied into the dental acrylic chamber above the motor cortex for ~30 min. Since epidural administration of water-soluble small drug molecules penetrate ~ 1.3 mm into the cortex within 15 min (Ludvig et al., 2008), I thought that 30 min infiltration is considered sufficient to block receptors in the M1. A recovery experiment was performed after the application of CNQX by continuously rinsing the exposed cortical surface with ACSF for 2 h during recovery.

Corpus callosum transection

The part of the corpus callosum (CC) that interconnects bilateral motor regions was transected using a wire knife (n = 4 animals). A guide cannula whose tip was curved in the caudal direction was positioned between bilateral olfactory bulbs, and a wire (φ = 0.3 mm) was inserted through the cannula along the midsaggital plane such that it was positioned between the midsaggital sinus and CC (Fig. 16A). The wire knife was gradually advanced ventrally, while verifying the VTA-evoked contralateral M1 response using a surface ball electrode. I found that it was sufficient to transect the dorsal part of the CC to eliminate the contra-M1 response (Fig. 16B). This cutting procedure allowed us to record evoked neuronal activity without massive bleeding from the midsagittal sinus. I confirmed that there was no damage to the underlying brain tissue by Nissl staining.

Histology

At the end of the experiment, animals were deeply anesthetized with pentobarbital (i.p.) and transcardially perfused with 4% paraformaldehyde. The brain was removed, post-fixed in the same fixative for over 24 h, and immersed in 0.1 M phosphate buffered saline (PBS) containing 30% sucrose until they sunk. The brain was cut into 30-μm thick coronal sections using a freezing microtome (Leica SM 2000R, Leica Microsystems,

Nussloch, Germany). The collected sections were processed for Nissl staining. Images of Nissl-stained sections were captured with a digital microscope (BZ-8100, Keyence, Osaka, Japan).

Immunohistochemistry

Coronal sections collected from the midbrain and M1 were used for tyrosine hydroxylase (TH) immunohistochemistry to stain DA cells. Sections were rinsed in 0.1 M PBS, non-specific binding was blocked by 2% normal goat serum with 0.1% Triton X-100 in 0.1 M PBS for 60 min, and then incubated with an anti-TH rabbit monoclonal antibody (1:1,000; Chemicon, Temecula, CA, USA) at 4^{o}C overnight. After washing three times with 0.1 M PBS, the sections were incubated with a biotinylated goat anti-rabbit IgG secondary antibody (1:500; PK-4001, Vector Laboratories Inc., Burlingame, CA, USA) at room temperature for 1 h, rinsed three times with 0.1 M PBS, and incubated with the avidin-biotin complex (PK-4001, Vector Laboratories Inc.) for 1 h. Staining was achieved by incubation with 3,3'-diaminobenzidine (DAB) mixed with distilled water, buffer pH 7.5, H_2O_2, and Nickel stock solution (SK-4100, Vector Laboratories Inc.). After staining with DAB, sections were washed in distilled water, mounted onto slides, dehydrated, cleared in xylene, and coverslips were added with mounting medium. Images of TH-stained

tissues were captured with a microscope (BZ-8100, Keyence). The density of stained tissues was analyzed using ImageJ software (developed at the National Institutes of Health) by quantifying the optical density within the VTA. Optical densities were normalized by subtracting the non-specific background staining. The optical density of TH-positive tissues in the lesioned-VTA was calculated relative to the intact VTA.

I also verified the DA fibers in M1 using TH immunofluorescence staining. The staining procedure was the same as that described above, except that anti-TH mouse monoclonal (1:1,000; Life Technologies) and Alexa Fluor 488-conjugated goat anti-mouse IgG (1:1,000; Life Technologies) antibodies were used as the primary and secondary antibodies, respectively. Coverslips were mounted using Fluoromount (DBS, Pleasanton, CA, USA). After capturing fluorescence images, the coverslips were removed in 0.1 M PBS, and Nissl staining was performed to identify the cortical layers.

Results

Neuronal activity in the M1 after VTA stimulation

VSD imaging was performed in the motor cortex to elucidate the spatiotemporal dynamics of neuronal activity after VTA stimulation (Fig. 6A). A representative example of the activity pattern of the optical signal is shown in Fig. 6B. Single pulse electrical stimulation (150 μA for 300 μs) of VTA-induced excitatory neuronal activity in the motor cortex began 13.3 ± 1.3 ms [mean ± standard error (SEM), n = 10] after stimulus onset. In the following ~ 20 ms, the cortical depolarization spread throughout the motor area. The excitatory response began to decrease ~ 30 ms after the stimulus onset and completely disappeared ~ 80 ms post-stimulation. Subsequent to the excitatory response, inhibitory neuronal activity developed for 379.4 ± 10.1 ms, covering a cortical area similar to where the previous excitatory response was observed. Fig. 6C shows an example of simultaneously recorded optical signal (upper traces) and LFP (lower traces). Cortical depolarization (upward deflection of optical signal) was evoked at the corresponding timing to downward deflection of the LFP, whereas cortical hyperpolarization was not clearly observed in the voltage signal. The peak amplitude and half-width (duration at half of peak amplitude) of excitatory and inhibitory responses were assessed for the 25–150 μA stimulus current in one rat based on the VSD imaging results (Fig. 7A). The

excitatory signal amplitude significantly increased with increasing stimulus intensity (25 μA vs. 150 μA stimulus current, –0.063 ± 0.015% vs. –0.149 ± 0.018%, $p < 0.01$), while only a slight increase was observed in the inhibitory signal amplitude (25 μA vs. 150 μA stimulus current, 0.096 ± 0.009% vs. 0.125 ± 0.021%, $p > 0.05$) (Fig. 7B). The excitatory response exhibited constant half-width duration irrespective of the stimulus intensity (25 μA vs. 150 μA stimulus current, 14 ± 2.6 ms vs. 14 ± 1.6 ms); however, the half-width was prolonged in the inhibitory response when a stronger stimulus was applied to the VTA (25 μA vs. 150 μA stimulus current, 258.5 ± 15.1 ms vs. 307.2 ± 14.7 ms, $p < 0.05$) (Fig. 7C). The stimulation site was histologically identified referring to the anatomical landmarks. Fig. 8A shows an example of Nissl-stained midbrain coronal section with electrolytic lesion at the stimulation site. The location of the stimulation sites selected from the 24 animals, either evoked (red circles, n=20) or fail to evoked (blue crosses, n=4) M1 response, are shown in Fig. 8B. Most of the stimulation sites that successfully generated the M1 activity were identified within or near the VTA and SNc.

Since DA neurons in the SNc also project to the M1 (Hosp et al., 2011), I examined M1 activity after the pulse stimulation (150 μA for 300 μs) of the SNc (n = 3). Fig. 9A shows an example of TH-stained midbrain section with three electrolytic marker lesions (a-c), which located within the VTA (a) and SNc (b-c). Activity pattern of VSD response

and optical signal traces are shown in Fig. 9B and 9C, respectively. After the SNc stimulation (“b” and “c” in Fig. 9B and 9C), excitatory-inhibitory sequence of neuronal activity was evoked in M1 with similar time course to the VTA-evoked response (“a” in Fig. 9B and 9C). Although small number of animals was used, this result suggested that there were no clear difference of optical signals in M1 activity between VTA and SNc stimulation. Thus, I focused only on VTA-evoked M1 response in the following experiments.

Relationship between motor representations and VTA-evoked response

I observed that the excitatory neuronal activity first appeared in the caudolateral part of the motor cortex, after which the activity extended into the rostromedial direction in all animals (data from 10 selected animals are shown in Fig. 10A). Thus, I confirmed motor representations in the optically mapped cortical area immediately after the VSD imaging experiments using an ICMS technique (n = 3). Fig. 10B shows an example of motor representations merged with the VSD imaging results. The location of motor representations was consistent with a previous study (Gioanni and Lamarche, 1985); a minimum movement threshold was 10 μA in the jaw area and 5 μA in both forelimb and vibrissae areas. Based on ICMS maps from the three animals, three ROIs were placed

over the motor cortex: CFA, RFA, and vibrissae motor area (Vib) (Fig. 10C). The amplitude and peak latency of the excitatory optical signal were compared among these areas (Fig. 10D and 10E). Fig. 10D shows that both the CFA and RFA were strongly activated with similar amplitudes [RFA, 0.657 ± 0.018; CFA, 0.653 ± 0.017 $(\Delta F/F)_{norm}$], while Vib activation was significantly weaker [0.36 ± 0.019 $(\Delta F/F)_{norm}$, $p < 0.01$]. Analysis of latency-to-peak effect indicated that the optical signal in CFA peaked 23.8 ± 0.8 ms after VTA stimulation, which was significantly faster than those in RFA (27.8 ± 0.46 ms, $p < 0.01$) and Vib (29.8 ± 1.0 ms, $p < 0.01$) (Fig. 10E). These results suggest that the VTA-evoked response first appears in the CFA and spreads toward the RFA.

The possibility that the CFA activity propagate to the RFA was assessed by performing the VSD imaging in motor cortex after the electrical stimulation of the CFA. Fig. 11A shows an activity patterns of the cortex in response to the CFA stimulation (50-150 μA, 200μs) at the depth of 500, 1000 and 1500 μm from the cortical surface (n = 3). Forelimb motor areas were mapped by ICMS after the VSD imaging (Fig. 11C). Electrically-evoked CFA activity started from the stimulation site immediately after the pulse stimulation, and then it extend to the RFA (Figs. 11A and 11C). The time contour maps in Fig. 11B show the extent of cortical area where optical signal amplitude exceeding the half maximum. The contour maps showed that the higher optical response

was corresponded to the CFA and the RFA (Figs. 11B and 11C). Although above activity pattern was observed in each stimulus condition, the most prominent and widespread cortical activity was evoked when the stimulation was applied to the depth of 1500 μm from cortical surface. Fig. 11D shows the optical signal traces selected from the CFA and the RFA. When stimulus current was applied to deeper cortical layers, slower rising phase of optical response was observed in the CFA (lower traces in Fig. 11D), but it evoked faster RFA activity (upper traces in Fig. 11D). The peak latency difference between the CFA and the RFA was significantly shorter in the deeper cortical layer stimulation (1000μm, 7 ± 2; 1500 μm, 5 ± 1 ms, $p < 0.05$) than upper layer stimulation (500 μm, 13 ± 1 ms) (Fig. 11E). These results suggest possibility that neuronal activity of the CFA after VTA stimulation might be transmitted to the RFA. The CFA and the RFA are thought to be equivalent to the M1 hand area and the premotor/supplementary motor area in primates, respectively (Rouiller et al., 1993).

Pharmacological effect on evoked response

VSD imaging of VTA-evoked neuronal activity was performed after the topical application of the non-NMDA glutamate receptor antagonist CNQX, the $GABA_A$ receptor antagonist bicuculline, or the D1/D2 type DA receptor antagonists (SCH 23390 and

sulpiride). Fig. 12A shows an example of the evoked activity before (upper panels) and after (lower panels) the application of CNQX. Both the excitatory and inhibitory neuronal activities were completely blocked after CNQX application. Partial recovery was observed after 2 h of washout (Fig. 12A, upper right panels). Fig. 12B shows the result before (upper panels) and after (lower panels) the application of bicuculline. Bicuculline enhanced the excitatory neuronal activity, with 3-fold larger peak amplitude of the optical signal compared with that of the control. On the contrary, the inhibitory neuronal activity completely disappeared after bicuculline treatment. Fig. 12C shows the effect of DA receptor antagonists on the VTA-evoked response. Blocking the DA receptors had no effect on excitatory-inhibitory neuronal activity. These results confirmed that VTA-evoked excitatory and inhibitory responses are elicited by glutamate and GABA, respectively. Furthermore, it is also suggested that GABAergic inhibitory M1 activity after VTA stimulation is caused by glutamate input to the M1.

The effect of 6-OHDA lesioning of DA neurons

To investigate the contribution of DA neurons in the neuronal activities of the M1, VSD imaging was applied to unilateral 6-OHDA-lesioned rats (n = 8). Firstly, I examined the distribution of DA terminals within the M1 of the control animals. In the normal M1, TH-

positive fibers were prominent in deep cortical layers, but were detected in all other layers (Fig. 13). After unilateral 6-OHDA treatment, TH-stained sections were collected from the VTA and M1. Histological examples of VTA and M1 sections are shown in Fig. 14B and 14C, respectively. Densitometry confirmed significantly less TH-staining in the 6-OHDA-treated VTA compared with the intact side (the density ratio of lesioned/intact VTA was 0.29 ± 0.13, $p < 0.01$, $n = 6$) (Fig. 14B). Immunofluorescence staining also showed a reduction in TH-positivity in the 6-OHDA-lesioned side of M1 deep layers (Fig. 14C). VSD imaging revealed that single-pulse stimulation of the lesioned VTA did not evoke any neuronal activities in M1 (Fig. 14D, upper panels). This result indicates that the VTA-evoked response in M1 originates from DA neurons in the VTA. I routinely applied electrical stimulation to the contralateral forelimb (VTA-intact side) to confirm whether there was the sensorimotor response in the imaged cortex (Figs. 14A and 14D, lower panels). The forelimb stimulation (600 μA, 1 pulse/ms) activated the caudolateral part of the imaged cortex, suggesting that this area was maintained as physiologically good condition to record optical signals (Fig. 14D, lower panels).

Bilateral M1 response after unilateral VTA stimulation

I investigated whether unilateral VTA stimulation activates the contralateral motor area,

the opposite hemisphere of the stimulus side. VSD imaging was performed in the bilateral M1 with a single pulse stimulation to the VTA (n = 6 animals, Fig. 15A). Electrical stimulation of the VTA elicited neuronal activity not only in the ipsilateral but also in the contralateral M1 (Fig. 15B). The contralateral M1 response spread from caudolateral toward rostromedial neurons (Fig. 15C), which resembled the ipsilateral M1 response (Fig. 10A). The contralateral response appeared later than did the ipsilateral response in all animals, and the delay in peak latency was 11.7 ± 0.7 ms (n = 6) between the optical signals at the symmetrical coordinates of each hemisphere (Fig. 15D). Fig. 15E shows that the peak amplitude of the optical signal was smaller in the contralateral than the ipsilateral M1 [contralateral, 0.559 ± 0.055; ipsilateral, 0.646 ± 0.069 $(\Delta F/F)_{norm}$]. Next, I injected the $GABA_A$ receptor agonist muscimol into the ipsilateral cortex with three to four penetrations (Fig. 15A). Muscimol injection into the ipsilateral M1 completely abolished the VTA-evoked activities in this side of the M1, but the neuronal activity in the contralateral M1 was sustained (Fig. 15F). These results indicate that the contralateral M1 response was not mediated by ipsilateral M1 neuron activity.

The effect of corpus callosum transection on contralateral M1 response

To assess whether contralateral M1 activity was transmitted through the interhemispheric

connection to ipsilateral M1, I transected the CC between M1 areas. Before and after CC transection, VTA-evoked M1 activity was measured by VSD imaging (Fig. 16A). Nissl-stained sections showed that the CC was transected without damage to the underlying brain structures (Fig. 16B). Before CC transection, unilateral right-VTA stimulation induced neuronal responses in both the ipsilateral (right) and contralateral (left) M1 (Fig. 16C). After CC transection, even though the VTA-evoked response in the right M1 (ipsilateral to the stimulated VTA) remained intact (Fig. 16D, upper panels), the neuronal activity in the left M1 (contralateral to the stimulated VTA) completely disappeared (Fig. 16D, middle panels). To determine whether the impaired response in the left M1 was due to loss of the CC connections, I stimulated the left-VTA and then confirmed that there was a normal ipsilateral response in the left M1 (Fig. 16D, lower panels).

M1 layers receiving synaptic inputs after VTA stimulation

I conducted CSD analysis in the M1 to elucidate the laminar localization of synaptic inputs from the VTA (n = 4 animals). Laminar field potentials were recorded using 16-channel silicon probes in the bilateral M1, in response to unilateral VTA stimulation. An example of voltage traces and CSD profiles are shown in Fig. 17. In the M1 ipsilateral to the stimulated VTA, CSD analysis revealed three current sinks in layers 2/3, 5, and 6

immediately after the stimulation (Fig. 17B). The earliest sink appeared in upper layer 5 and peaked 25.9 ± 1.9 ms after the stimulus onset. Subsequently, another weak sink was observed in layer 6. The other current sink in layer 2/3 showed a peak latency of 28.3 ± 1.3 ms, which was significantly delayed from the first sink ($p < 0.01$). The laminar CSD profile of the M1 response contralateral to the stimulated VTA was similar to that of the ipsilateral response (Fig. 17C), although the amplitudes of all current sinks largely decreased.

The effect of 6-OHDA lesioning on contralateral M1 response

Using 6-OHDA-lesioned rats (n = 6 animals), I investigated the contribution of DA neurons in generating the contralateral M1 response. The VTA was lesioned unilaterally, and then VSD imaging was performed in the contralateral M1 after stimulation of the intact or lesioned VTA (Fig. 18A). An example of a TH-stained section is shown in Fig. 18B: the ratio of TH-positive neurons was 20% or less, and electrolytic lesions indicate the stimulated sites. VSD imaging revealed that electrical stimulation to the lesioned side of the VTA did not produce any neuronal response in the contralateral M1; however, typical excitatory-inhibitory neuronal activity was observed in this cortex when the intact VTA side was stimulated ipsilaterally (Fig. 18C). These results suggest that the

contralateral M1 response, as well as the ipsilateral M1 response (see Fig. 14), arises from VTA-DA neurons.

Paired-stimulation between the M1 and VTA

Finally, I investigated how VTA stimulation modulates M1 excitability when a motor command is generated. Here I used a pair-pulse stimulation protocol, in which ICMS to M1 was paired with VTA stimulation (Fig. 19A). The ICMS-evoked motor output was evaluated by recording upper limb muscle EMG. In the first situation, I verified that neither VTA stimulation nor M1 ICMS produced EMG activity (Fig. 19B and 19C) before applying the paired-pulse stimulation. Even though the intensity of ICMS was adjusted to just below the movement threshold, the under-threshold ICMS successfully elicited the EMG response when associated with VTA stimulation (Fig. 19D). The VTA stimulation was applied 10 ms before the ICMS in Fig. 19D, because the result of VSD imaging indicated that the VTA-evoked excitatory response in the M1 started to evolve 10 ms post-stimulation (Fig. 6B and 6C). In the second situation, the VTA stimulation was applied under the condition that M1 stimulation just above the movement threshold resulted in reproducible EMG responses (Fig. 19E). Then, I increased the inter-stimulus interval (ISI) between VTA-M1 pairs and found that the ICMS-evoked EMG was

completely suppressed when the ISI was 30 ms (Fig. 19F). The EMG response reappeared when ISI was longer than 40 ms, and was restored to control levels in 100–200 ms (Fig. 19G–I). Strong EMG suppression was reliably observed during the narrow time window when the conditioning VTA stimulation was preceded by 30–50 ms. These results suggest that motor output from M1 is facilitated or inhibited, depending on the timing of VTA activation. To explain the time window of the EMG suppression by the preceding VTA stimulation, I calculated the time derivative of the VTA-induced optical signal (Fig. 19J). This is because Eriksson et al. (2008) demonstrated that the time derivative of the VSD signal was strongly correlated with the stimulus-evoked changes in the firing rate of neurons. As shown in Fig. 19J, the time derivative signal was largely negative at 30–50 ms post-stimulation, suggesting that the driving force of inhibition was stronger during this time window.

Although EMG results show that VTA-evoked M1 activity modulate muscle activity with time-dependent manners, it is unclear whether ICMS-evoked M1 activity is modulated by VTA stimulation. To address this issue, M1 activity was measured by VSD imaging during paired-stimulation of VTA and M1, which is the same situation as in the EMG experiments (n = 1 animal, Fig. 20A). Example of optical signal traces and activation pattern with or without paired stimulation were shown in Fig. 20B and 20E-L,

respectively. When VTA and M1 stimulation were paired with 10-15ms ISI, the depolarizing components of the optical signal overlapped each other, as a result, the peak amplitude of the signal enhanced (Fig. 20B and 20G-H) comparing to the peak amplitude after VTA stimulation without paring (Fig. 20F). When the ISI was longer than 30 ms, two peaks in the optical signal were distinguished, each of which was originated by VTA or M1 stimulation, respectively (Fig. 20B). The M1-ICMS response was suppressed at the ISI of 30-50 ms but recovered at the ISIs longer than 100 ms (Fig. 20B), as was observed in EMG results (Fig. 19). Modulatory effect of the paired stimulation was analyzed by counting the number of pixels, at which the signal amplitude exceeding a certain threshold (Fig. 20C and 20D). This analysis confirmed that larger number of pixels overcome the certain threshold than control activity when VTA and M1 stimulation was paired with ISI of 10-15ms, while it decreased when M1-ICMS was applied 30-50ms after the VTA stimulation. These results suggest that ICMS-evoked M1 activity is modulated by VTA stimulation similar to the EMG results.

Discussion

The present study is the first report of the M1 neuronal activity in response to single pulse electrical stimulation to the VTA. VSD imaging revealed that the stimulation of the unilateral VTA elicited a short-latency excitatory and inhibitory sequence of neuronal activity in both sides of M1. The combination of VSD imaging and motor mapping clarified that the VTA-evoked response was especially prominent in the forelimb areas. The M1 response (both excitatory and inhibitory activity) completely disappeared by 6-OHDA-lesioning of the VTA, and by blocking the glutamate receptor in the intact M1. Furthermore, the VTA-induced M1 response modulated M1 outputs with time-dependent manners.

Midbrain DA neurons evoke an excitatory-inhibitory neuronal response

Although a short-latency neuronal response after DA neuron activation was reported in the PFC (Mercuri et al., 1985; Lavin et al., 2005; Watanabe et al., 2009), here I showed the first evidence of a short-latency response in the M1, as characterized by an excitatory-inhibitory sequence (Fig. 6). The optically detected M1 response peaked ~30 ms after the VTA stimulation, and was blocked by a glutamate receptor antagonist but not by DA receptor antagonists (Fig. 12). Furthermore, stimulation of the VTA after the 6-OHDA

lesioning failed to evoke M1 responses (Figs. 14 and 18). My findings in the M1 are consistent with previous observations in the PFC, suggesting that the M1 and PFC share certain characteristics common to the mesocortical DA projection system. It is not improbable that the observed M1 response might include the antidromic activation of M1 neurons. However, this possibility seems negligible because M1 response was not evoked in VTA-lesioned animals (Fig. 14). In addition, effective stimulation sites were located within the VTA/SNc (Fig. 8), indicating that the fast-M1 response originated from these midbrain areas.

What type of VTA-neurons are involved in the short-latency M1 response? There are two possibilities: (1) DA neurons and (2) glutamate neurons in the VTA. In the former case, glutamate, which is coreleased with DA from DA neurons, might play critical role in well-timed signal transmission. Although it seems improbable that the VTA-glutamate neurons produce the excitatory M1 response since 6-OHDA is one of the most commonly used neurotoxin for degeneration of DA neurons (Beal, 2001; Schober, 2004), a previous report suggests that the 6-OHDA destroys both DA and non-DA VTA neurons depending on the drug concentration (Michel et al., 1990). Thus, it remains a possibility that the 6-OHDA destroy non-DA neurons that might be involved in carrying the fast signals to the cortex (Gorelova et al., 2012). Another possible origin of the fast response observed in

the present study is the VTA-glutamate neurons. Yamaguchi et al. (2011) showed that the PFC projecting VTA neurons are composed of VGLUT2 mRNA expressing glutamate neurons (~40%), VGLUT2 mRNA and TH co-expressing neurons (~30%), TH positive DA neurons (~20%) and a few of VGLUT2 and TH negative neurons (presumably GABA neurons) (~10%). Using optogenetic methods, Hnasko et al. (2012) revealed that the activation of VGLUT2 expressing VTA neurons evoked fast glutamate response in the NAc and ventral pallidum. Since ventral pallidum is not known to receive DA input, they concluded that the VTA-glutamate neurons generated fast signal in ventral pallidum (Hnasko et al., 2012). However, because it was indicated that only a few (2-3%) VTA neurons expressed VGLUT2 mRNA (Nair-Roberts et al., 2008), further anatomical and physiological evidences are needed to determine whether VTA-glutamate neurons induce fast signal in the cortex.

Considering the previous electrophysiological studies in the PFC, both non-DA and DA components was reported in the VTA-evoked short latency neuronal response (Thierry et al., 1980; Gariano et al., 1989). Thierry et al., (1980) classified the short-latency PFC response into two components by analysis of antidromic activity; one was conduction velocity of 3.2 m/s and not affected by 6-OHDA lesion of the VTA, the other was conduction velocity of 0.55 m/s and largely disappeared by 6-OHDA treatment.

Because DA fiber in the rat has approximately 0.5-0.6 m/s conduction velocity (Rodriguez and Gonzalez-Hernandez, 1999), slower component in the fast response can be induced by DA projection (Lapish et al., 2007). In the present study, when assuming that the conduction velocity of DA fiber is 0.55 m/s, the response latency elicited in M1 can be estimated as 18 ms after the stimulation of the VTA, which is 10 mm apart from M1. Nevertheless, this expected latency is somewhat longer than the present imaging result (Fig. 6). This difference may be caused by the method of investigation: VSD signal mainly reflect synaptic potential, while conduction velocity of DA fiber was estimated from the action potentials (Gariano et al., 1989; Lapish et al., 2007). Therefore, it seems reasonable to conclude that the M1 response observed in the present study was mediated by corelease of glutamate from DA pathway. However, the possibility that the pathway for short-latency signal transmission might be different between VTA-PFC and -M1 cannot be ruled out by the present data. VTA neurons project many brain areas, and then some of these areas project directly and/or indirectly to the M1 (Swanson, 1982; Ikemoto, 2007; Redgrave et al., 2010). Thus short-latency M1 response could be transmitted from the VTA to the M1 through the indirect pathway(s). Overcome these issues, future studies should incorporate techniques that can selectively manipulate the activity of DA and non-DA projection, such as the optogenetic methods.

Following the excitatory response, VTA stimulation induced an inhibitory response for ~ 400 ms (Fig. 6). The VTA-evoked inhibitory neuronal response was blocked by both GABA and glutamate receptor antagonists (Fig. 12). Therefore, the inhibitory activity could be produced by GABAergic interneurons in the M1 via glutamate neurotransmission, rather than a direct GABAergic projection from the VTA as reported previously in the VTA-PFC pathway (Carr and Sesack, 2000). I hypothesized that M1 pyramidal neurons during this inhibitory period were strongly inhibited, and had become difficult to fire. However, the ICMS-evoked motor cortical activity and its output were easily produced in this inhibitory period. In contrast, suppression of motor output was observed during the narrow time window when the VSD signals shifted rapidly from excitatory to inhibitory (Fig. 19 and 20). Although the inhibitory map of VSD imaging suggests that the inhibitory synaptic activities are predominant during this period, it does not directly demonstrate the strength of inhibition to the pyramidal neurons in that area (Eriksson et al., 2008). As Eriksson et al. suggested, if I assume that the firing dynamics of pyramidal neurons is correlated with the time differential values of the VSD signals, it might well explain the existence of the short suppression period (Figs. 19 and 20). Practically, firing activity of the PFC pyramidal neurons is decreased after VTA activation simultaneously with increase of interneuron firing (Tseng et al., 2006). Thus, pyramidal

neurons in the M1 could receive inhibitory synaptic input after the VTA stimulation, which might make M1 neurons difficult to fire. The sequential activation of multiple interneuron types within the M1 may give rise to short-term suppression of M1 output and long-lasting inhibition (Apicella et al., 2012).

The forelimb motor area is the major target of activation

The VSD imaging followed by ICMS mapping successfully demonstrated that the VTA-evoked response was stronger in the forelimb areas of the motor cortex (Fig. 10). This observation is consistent with reports by Hosp et al. (2009, 2011), who indicated that VTA-M1 DA projections help improve forelimb motor learning and extend the size of forelimb motor representation. The VTA-evoked M1 response appeared from the CFA, and then propagated to the RFA (Figs. 10 and 11). These observations are consistent with previous anatomical finding that the RFA receives strong projections from the CFA layer 2/3 and/or layer 5a (Hira et al., 2013). According to my CSD analysis, the M1 receives synaptic inputs in upper layer 5 and then layer 2/3 and 6 successively after VTA stimulation (Fig. 17). Therefore, the VTA likely sends a neuronal signal first to the CFA, and thereafter, some processed information is relayed to the RFA via cortico-cortical connections.

In the present CSD analysis revealed that the first current sink, presumably reflecting the excitatory synaptic inputs, occurred in upper layer 5. However, the densest DA fibers were distributed in the layer 6 (Fig. 13). This discrepancy may be due to the existence of two classes of DA terminals: typical synaptic and varicose-like terminals (Descarries et al., 2008). The synaptic DA terminals are hypothesized to be used for glutamate corelease, while the DA-containing varicosities accomplish volume transmission of DA (Trudeau et al., 2004). Since the two types of DA terminals can be located at sites distant from each other, it is not surprising that the M1 receives fast signals from VTA in its upper layer 5 via synaptic DA terminals. This idea parallels the observation that intense VGLUT2-immunopositive staining is densely localized in rat layer 4 and superficial 5 (Kaneko et al., 2002). Weak current sink observed in layer 6 might imply that the amount of synaptic DA terminals in layer 6 is smaller than VGLUT2 expressing synaptic terminals in upper layer 5.

Parallel activation of the bilateral M1

Unilateral VTA stimulation induced an excitatory-inhibitory sequence of neuronal activity in the bilateral M1 (Fig. 15). It would be expected that the evoked response in the contralateral hemisphere is mediated by the ipsilateral M1 because rich commissural

connections between motor areas have been identified (Donoghue and Parham, 1983). However, my VSD imaging with pharmacological treatment showed that the contralateral M1 response occurred irrespective of the presence of ipsilateral M1 activation (Fig. 15). Furthermore, CSD analysis revealed that the contra- and ipsilateral M1 responses had similar depth profiles (Fig. 17). These results suggest that the stimulation of the unilateral VTA drives bilateral M1 activation via parallel projections. In the present data, the time difference between the ipsi- and contra-M1 responses was approximately 12ms. When conduction velocity is assumed to be 0.55 m/s, as discussed above, latency difference is 12 ms between the M1s, which is apart from about 6.6 mm (Paxinos and Watson, 1998). The possibility of parallel projection is supported by the anatomical findings of Hosp et al. (2011), who injected a retrograde tracer into the forelimb area of the M1 and reported that 12% of retrogradely labeled DA neurons were located in the contralateral VTA. One could speculate that the DA projections to the contralateral hemisphere may be used for compensation in the case of unilateral VTA damage. This notion comes from the observation that a unilateral VTA lesion facilitates the activity in the opposite side of the intact VTA (Trojniar and Staszewska, 1994; Majkutewicz et al., 2010).

Functional significance of fast signaling

According to conventional theories of DA reward signaling, the phasic activity of VTA-DA neurons encodes temporally precise information about reward or reward predictions, and then this information is transmitted to reward-related brain areas (Schultz, 1998, 2007). Roesch and Olson (2003) reported strong reward-related activity of premotor neurons in monkeys performing a memory-guided saccade task, and concluded that this might be attributable to the monkey's motivation level. My findings showing the presence of fast signaling from the VTA to the M1 suggest that the reward signals could be exploited at the most downstream processing of motor output. Since evoked-M1 activity was prominent in the forepaw areas, I predict that the VTA-to-M1 signal is operative when rats struggle to perform skill- and dexterity-based movements (e.g., manipulating small food with their paws). A recent study by Thabit et al. (2011) also supports this idea, as they reported that the money reward modulated the excitability of the human M1.

The contribution of VTA-M1 projections to motor skill learning was impressively demonstrated by Hosp et al. (2011). They showed that motor skill learning was impaired after VTA lesion by 6-OHDA, but learning impairment was significantly, but partially, rescued by levodopa administration; success rate of reaching task was recovered to approximately half of the control animals (Hosp et al., 2011). Thus, in addition to the DA,

another factor might be required to acquire the fine motor skills. In my paired stimulation studies, VTA-evoked cortical excitation facilitated M1-evoked cortical activity and EMG response (Figs. 19 and 20). These results suggest that VTA activation increases firing probability of M1 neurons that follows excitatory synaptic inputs from other brain areas, e.g. motor related brain areas. Because synaptic connectivity is strengthened when postsynaptic neurons fired shortly after the presynaptic neural firing (Froemke and Dan, 2002), the efficacy of synaptic inputs from motor related brain areas to the M1 would be improved if VTA increases M1 excitability in advance. Strengthening of synaptic connectivity was further promoted by DA when applied within 0.3 to 2 seconds after glutamatergic inputs in the NAc (Yagishita et al., 2014), although DA concentration in the M1 after VTA activation is still unknown. Thus, glutamate and DA released from the VTA-M1 pathway may cooperate to enhance synaptic connectivity in the M1.

Another possible role of glutamate in DA pathway is to promote the DA neurotransmission. The DA storage into the vesicular monoamine transporters was facilitated when glutamate was co-existed with DA in the same presynaptic terminal (Hnasko et al., 2010). Furthermore, co-existence of glutamate and DA promotes growth of DA axons (Schmitz et al., 2009). Thus, glutamate would contribute to DA neurotransmission and, consequently, facilitate plastic changes in target areas induced by

DA neurotransmission.

The motor execution is also controlled by VTA-evoked fast M1 response. Wang and Tsien (2011) showed the burst firing of VTA neurons at both the onset and the offset of voluntary wheel-running behavior in mice. Transient increase in M1 activity by the VTA neurons could help to drive motor output for movement initiation and termination. In addition to the locomotion, phasic activation of VTA neurons may help to trigger sudden movements related to reward-seeking behavior and escape reaction. In the PFC neurons, firing rate is increased immediately after the VTA activation (Lewis and O' Donnell, 2000; Seamans and Yang, 2004; Tseng et al., 2006), and the spontaneous activity synchronizes with VTA activity (Peters et al., 2004). Supposing similar modulatory effects in the M1, VTA changes M1 activity with temporally precise manner. The results of EMG experiments (Fig. 19), in which the VTA activation modulated (facilitated or inhibited) M1 output on a scale of several tens of milliseconds, could be explained in this context.

The importance of the long-lasting inhibition depicted by VSD imaging is unknown. The inhibitory response was not sufficient to abolish motor output (Fig. 19). However, I assumed that hyperpolarized membrane potential might reduce spontaneous M1 activity. When involved with motor learning, the VTA might slightly silence the M1 for several

hundreds of milliseconds to prepare for the succeeding generation of intended motor commands (Cohen and Sternad, 2009). Another possibility is that the inhibition might form the basis for generating synchronous activity in M1 neurons. Synchronous oscillations can be generated when inhibitory interneuron networks are activated (Beierlein et al., 2000). The possible synchronous activity in M1 that might encode information concerning motor learning, which could be transmitted to the dorsal striatum; the dorsal striatum is thought to play an important role in motor learning (Pennartz et al., 2009).

Future directions

Ascending DA pathways originating from the VTA and SNc are classically divided into two different types: the meso-cortico-limbic projection from the VTA to the cortex and NAc, and the nigro-striatal projection from the SNc to the dorsal striatum. This widely used rough classification has been helpful for understanding the pathogenesis of several diseases, such as addiction and Parkinson's disease. However, this traditional dichotomous is insufficient because the M1 receives DA projection from both VTA and SNc in the rat, as well as in the monkey (Hosp et al., 2011; Williams and Goldman-Rakic, 1998). In the preliminary data in this study, electrical stimulation of the SNc evoked an

excitatory-inhibitory sequence of neuronal response in the M1 with quite similar spatiotemporal pattern to the VTA-evoked response (Fig. 9). This result suggests that widely distributed cell populations in the VTA/SNc transmit fast signal to the M1. Further investigation to reveal the difference between VTA- and SNc-M1 pathway will help us to advance our understanding of the role of these regions.

Finally, the present results were obtained by electrically-evoked neuronal activation in the anesthetized rats. Further studies linking these data to behavioral experiments are necessary to elucidate functional roles of fast signaling from midbrain DA neurons to the M1, and to investigate the potential impact of exploiting this signal pathway during rehabilitation of motor deficits.

Conclusion

The present study revealed that the VTA transmits fast signal to the bilateral M1. As a result of VTA activation, excitatory and inhibitory M1 response was generated by glutamate and GABA, respectively. The fast signal from the VTA to the M1 might be used for immediate transmission of DA neuronal activities related to reward and salient non-reward stimuli. The current results could be important because they demonstrate that VTA-neurons transmit the fast signal to the last cortical stage of motor command processing. Using the fast signal, VTA neurons could help to trigger and modulate the movements for adapting them to the optimal goal-directed behavior in a temporally precise manner.

References

Apicella AJ, Wickersham IR, Seung HS, Shepherd GMG (2012) Laminarly Orthogonal Excitation of Fast-Spiking and Low-Threshold-Spiking Interneurons in Mouse Motor Cortex. J Neurosci 32:7021-7033.

Bao S, Chan VT, Merzenich MM (2001) Cortical remodelling induced by activity of ventral tegmental dopamine neurons. Nature 412:79-83.

Beal MF (2001) Experimental models of Parkinson's disease. Nat Rev Neurosci 2:325-334.

Beierlein M, Gibson JR, Connors BW (2000) A network of electrically coupled interneurons drives synchronized inhibition in neocortex. Nat Neurosci 3:904-910.

Berger B, Gaspar P, Verney C (1991) Dopaminergic Innervation of the Cerebral-Cortex - Unexpected Differences between Rodents and Primates. Trends in Neurosciences 14:21-27.

Berger B, Verney C, Alvarez C, Vigny A, Helle KB (1985) New Dopaminergic Terminal Fields in the Motor, Visual (Area 18b) and Retrosplenial Cortex in the Young and Adult-Rat - Immunocytochemical and Catecholamine Histochemical Analyses. Neuroscience 15:983-998.

Bromberg-Martin ES, Matsumoto M, Hikosaka O (2010) Dopamine in motivational

control: rewarding, aversive, and alerting. Neuron 68:815-834.

Carr DB, Sesack SR (2000) GABA-containing neurons in the rat ventral tegmental area project to the prefrontal cortex. Synapse 38:114-123.

Cisek P, Crammond DJ, Kalaska JF (2003) Neural activity in primary motor and dorsal premotor cortex in reaching tasks with the contralateral versus ipsilateral arm. J Neurophysiol 89:922-942.

Cohen RG, Sternad D (2009) Variability in motor learning: relocating, channeling and reducing noise. Exp Brain Res 193:69-83.

Dal Bo G, St-Gelais F, Danik M, Williams S, Cotton M, Trudeau LE (2004) Dopamine neurons in culture express VGLUT2 explaining their capacity to release glutamate at synapses in addition to dopamine. J Neurochem 88:1398-1405.

Descarries L, Berube-Carriere N, Riad M, Dal Bo G, Mendez JA, Trudeau LE (2008) Glutamate in dopamine neurons: Synaptic versus diffuse transmission. Brain Research Reviews 58:290-302.

Descarries L, Lemay B, Doucet G, Berger B (1987) Regional and Laminar Density of the Dopamine Innervation in Adult-Rat Cerebral-Cortex. Neuroscience 21:807-824.

Donoghue JP, Parham C (1983) Afferent connections of the lateral agranular field of the rat motor cortex. J Comp Neurol 217:390-404.

Drew T, Andujar JE, Lajoie K, Yakovenko S (2008) Cortical mechanisms involved in visuomotor coordination during precision walking. Brain Res Rev 57:199-211.

Eriksson D, Tompa T, Roland PE (2008) Non-linear population firing rates and voltage sensitive dye signals in visual areas 17 and 18 to short duration stimuli. PLoS One 3:e2673.

Esposito MS, Capelli P, Arber S (2014) Brainstem nucleus MdV mediates skilled forelimb motor tasks. Nature 508:351-356.

Froemke RC, Dan Y (2002) Spike-timing-dependent synaptic modification induced by natural spike trains. Nature 416:433-438.

Gariano RF, Tepper JM, Sawyer SF, Young SJ, Groves PM (1989) Mesocortical Dopaminergic-Neurons .1. Electrophysiological Properties and Evidence for Soma-Dendritic Autoreceptors. Brain Research Bulletin 22:511-516.

Garris PA, Wightman RM (1994) Different kinetics govern dopaminergic transmission in the amygdala, prefrontal cortex, and striatum: an in vivo voltammetric study. J Neurosci 14:442-450.

Gioanni Y, Lamarche M (1985) A reappraisal of rat motor cortex organization by intracortical microstimulation. Brain Res 344:49-61.

Gorelova N, Mulholland PJ, Chandler LJ, Seamans JK (2012) The glutamatergic

component of the mesocortical pathway emanating from different subregions of the ventral midbrain. Cereb Cortex 22:327-336.

Greenough WT, Larson JR, Withers GS (1985) Effects of unilateral and bilateral training in a reaching task on dendritic branching of neurons in the rat motor-sensory forelimb cortex. Behav Neural Biol 44:301-314.

Grinvald A, Hildesheim R (2004) VSDI: a new era in functional imaging of cortical dynamics. Nat Rev Neurosci 5:874-885.

Harms KJ, Rioult-Pedotti MS, Carter DR, Dunaevsky A (2008) Transient spine expansion and learning-induced plasticity in layer 1 primary motor cortex. J Neurosci 28:5686-5690.

Hira R, Ohkubo F, Tanaka YR, Masamizu Y, Augustine GJ, Kasai H, Matsuzaki M (2013) In vivo optogenetic tracing of functional corticocortical connections between motor forelimb areas. Front Neural Circuits 7:55.

Hnasko TS, Hjelmstad GO, Fields HL, Edwards RH (2012) Ventral Tegmental Area Glutamate Neurons: Electrophysiological Properties and Projections. J Neurosci 32:15076-15085.

Hnasko TS, Chuhma N, Zhang H, Goh GY, Sulzer D, Palmiter RD, Rayport S, Edwards RH (2010) Vesicular glutamate transport promotes dopamine storage and

glutamate corelease in vivo. Neuron 65:643-656.

Horvitz JC (2000) Mesolimbocortical and nigrostriatal dopamine responses to salient non-reward events. Neuroscience 96:651-656.

Hosp JA, Pekanovic A, Rioult-Pedotti MS, Luft AR (2011) Dopaminergic projections from midbrain to primary motor cortex mediate motor skill learning. J Neurosci 31:2481-2487.

Hosp JA, Molina-Luna K, Hertler B, Atiemo CO, Luft AR (2009) Dopaminergic Modulation of Motor Maps in Rat Motor Cortex: An in Vivo Study. Neuroscience 159:692-700.

Huber D, Gutnisky DA, Peron S, O'Connor DH, Wiegert JS, Tian L, Oertner TG, Looger LL, Svoboda K (2012) Multiple dynamic representations in the motor cortex during sensorimotor learning. Nature 484:473-478.

Ikemoto S (2007) Dopamine reward circuitry: two projection systems from the ventral midbrain to the nucleus accumbens-olfactory tubercle complex. Brain Res Rev 56:27-78.

Kakei S, Hoffman DS, Strick PL (1999) Muscle and movement representations in the primary motor cortex. Science 285:2136-2139.

Kaneko T, Fujiyama F, Hioki H (2002) Immunohistochemical localization of candidates

for vesicular glutamate transporters in the rat brain. J Comp Neurol 444:39-62.

Karni A, Meyer G, Rey-Hipolito C, Jezzard P, Adams MM, Turner R, Ungerleider LG (1998) The acquisition of skilled motor performance: fast and slow experience-driven changes in primary motor cortex. Proc Natl Acad Sci U S A 95:861-868.

Karni A, Meyer G, Jezzard P, Adams MM, Turner R, Ungerleider LG (1995) Functional MRI evidence for adult motor cortex plasticity during motor skill learning. Nature 377:155-158.

Kawano M, Kawasaki A, Sakata-Haga H, Fukui Y, Kawano H, Nogami H, Hisano S (2006) Particular subpopulations of midbrain and hypothalamic dopamine neurons express vesicular glutamate transporter 2 in the rat brain. J Comp Neurol 498:581-592.

Kleim JA, Hogg TM, VandenBerg PM, Cooper NR, Bruneau R, Remple M (2004) Cortical synaptogenesis and motor map reorganization occur during late, but not early, phase of motor skill learning. J Neurosci 24:628-633.

Kleim JA, Barbay S, Nudo RJ (1998) Functional reorganization of the rat motor cortex following motor skill learning. J Neurophysiol 80:3321-3325.

Lapish CC, Kroener S, Durstewitz D, Lavin A, Seamans JK (2007) The ability of the mesocortical dopamine system to operate in distinct temporal modes.

Psychopharmacology (Berl) 191:609-625.

Lavin A, Nogueira L, Lapish CC, Wightman RM, Phillips PE, Seamans JK (2005) Mesocortical dopamine neurons operate in distinct temporal domains using multimodal signaling. J Neurosci 25:5013-5023.

Lawrence DG, Kuypers HG (1968) The functional organization of the motor system in the monkey. I. The effects of bilateral pyramidal lesions. Brain 91:1-14.

Lewis BL, O'Donnell P (2000) Ventral tegmental area afferents to the prefrontal cortex maintain membrane potential 'up' states in pyramidal neurons via D(1) dopamine receptors. Cereb Cortex 10:1168-1175.

Lindenbach D, Bishop C (2013) Critical involvement of the motor cortex in the pathophysiology and treatment of Parkinson's disease. Neurosci Biobehav Rev 37:2737-2750.

Ludvig N, Sheffield LG, Tang HM, Baptiste SL, Devinsky O, Kuzniecky RI (2008) Histological evidence for drug diffusion across the cerebral meninges into the underlying neocortex in rats. Brain Res 1188:228-232.

Luft AR, Schwarz S (2009) Dopaminergic signals in primary motor cortex. Int J Dev Neurosci 27:415-421.

Majkutewicz I, Cecot T, Jerzemowska G, Myslinska D, Plucinska K, Trojniar W, Wrona

D (2010) Lesion of the ventral tegmental area amplifies stimulation-induced Fos expression in the rat brain. Brain Res 1320:95-105.

Masamizu Y, Tanaka YR, Tanaka YH, Hira R, Ohkubo F, Kitamura K, Isomura Y, Okada T, Matsuzaki M (2014) Two distinct layer-specific dynamics of cortical ensembles during learning of a motor task. Nat Neurosci 17:987-994.

Matsuda W, Furuta T, Nakamura KC, Hioki H, Fujiyama F, Arai R, Kaneko T (2009) Single nigrostriatal dopaminergic neurons form widely spread and highly dense axonal arborizations in the neostriatum. J Neurosci 29:444-453.

Matsumoto M, Hikosaka O (2009) Two types of dopamine neuron distinctly convey positive and negative motivational signals. Nature 459:837-841.

Mercuri N, Calabresi P, Stanzione P, Bernardi G (1985) Electrical stimulation of mesencephalic cell groups (A9-A10) produces monosynaptic excitatory potentials in rat frontal cortex. Brain Res 338:192-195.

Michel PP, Hefti F (1990) Toxicity of 6-hydroxydopamine and dopamine for dopaminergic neurons in culture. J Neurosci Res 26:428-435.

Middleton FA, Strick PL (2000) Basal ganglia output and cognition: evidence from anatomical, behavioral, and clinical studies. Brain Cogn 42:183-200.

Mitzdorf U (1985) Current source-density method and application in cat cerebral cortex:

investigation of evoked potentials and EEG phenomena. Physiol Rev 65:37-100.

Molina-Luna K, Pekanovic A, Rohrich S, Hertler B, Schubring-Giese M, Rioult-Pedotti MS, Luft AR (2009) Dopamine in Motor Cortex Is Necessary for Skill Learning and Synaptic Plasticity. Plos One 4:e7082

Nair-Roberts RG, Chatelain-Badie SD, Benson E, White-Cooper H, Bolam JP, Ungless MA (2008) Stereological estimates of dopaminergic, GABAergic and glutamatergic neurons in the ventral tegmental area, substantia nigra and retrorubral field in the rat. Neuroscience 152:1024-1031.

Nicholson C, Freeman JA (1975) Theory of current source-density analysis and determination of conductivity tensor for anuran cerebellum. J Neurophysiol 38:356-368.

Nishimura Y, Onoe H, Onoe K, Morichika Y, Tsukada H, Isa T (2011) Neural substrates for the motivational regulation of motor recovery after spinal-cord injury. PLoS One 6:e24854.

Nudo RJ, Milliken GW, Jenkins WM, Merzenich MM (1996) Use-dependent alterations of movement representations in primary motor cortex of adult squirrel monkeys. J Neurosci 16:785-807.

Paxinos and Watson (1998) The Rat Brain in Sterotaxic Coordinates. Academic Press 4th

ed.

Pennartz CM, Berke JD, Graybiel AM, Ito R, Lansink CS, van der Meer M, Redish AD, Smith KS, Voorn P (2009) Corticostriatal Interactions during Learning, Memory Processing, and Decision Making. J Neurosci 29:12831-12838.

Peters Y, Barnhardt NE, O'Donnell P (2004) Prefrontal cortical up states are synchronized with ventral tegmental area activity. Synapse 52:143-152.

Peters AJ, Chen SX, Komiyama T (2014) Emergence of reproducible spatiotemporal activity during motor learning. Nature 510:263-267.

Petersen CC, Grinvald A, Sakmann B (2003) Spatiotemporal dynamics of sensory responses in layer 2/3 of rat barrel cortex measured in vivo by voltage-sensitive dye imaging combined with whole-cell voltage recordings and neuron reconstructions. J Neurosci 23:1298-1309.

Redgrave P, Rodriguez M, Smith Y, Rodriguez-Oroz MC, Lehericy S, Bergman H, Agid Y, DeLong MR, Obeso JA (2010) Goal-directed and habitual control in the basal ganglia: implications for Parkinson's disease. Nat Rev Neurosci 11:760-772.

Rioult-Pedotti MS, Friedman D, Donoghue JP (2000) Learning-induced LTP in neocortex. Science 290:533-536.

Rioult-Pedotti MS, Friedman D, Hess G, Donoghue JP (1998) Strengthening of horizontal

cortical connections following skill learning. Nat Neurosci 1:230-234.

Rodriguez M, Gonzalez-Hernandez T (1999) Electrophysiological and morphological evidence for a GABAergic nigrostriatal pathway. J Neurosci 19:4682-4694.

Roesch MR, Olson CR (2003) Impact of expected reward on neuronal activity in prefrontal cortex, frontal and supplementary eye fields and premotor cortex. J Neurophysiol 90:1766-1789.

Rouiller EM, Moret V, Liang F (1993) Comparison of the connectional properties of the two forelimb areas of the rat sensorimotor cortex: support for the presence of a premotor or supplementary motor cortical area. Somatosens Mot Res 10:269-289.

Ruscher K, Kuric E, Wieloch T (2012) Levodopa treatment improves functional recovery after experimental stroke. Stroke 43:507-513.

Schmitz Y, Luccarelli J, Kim M, Wang M, Sulzer D (2009) Glutamate controls growth rate and branching of dopaminergic axons. J Neurosci 29:11973-11981.

Schober A (2004) Classic toxin-induced animal models of Parkinson's disease: 6-OHDA and MPTP. Cell Tissue Res 318:215-224.

Schultz W (2007) Behavioral dopamine signals. Trends Neurosci 30:203-210.

Schultz W (2002) Getting formal with dopamine and reward. Neuron 36:241-263.

Schultz W (1998) Predictive reward signal of dopamine neurons. J Neurophysiol 80:1-

27.

Seamans JK, Yang CR (2004) The principal features and mechanisms of dopamine modulation in the prefrontal cortex. Prog Neurobiol 74:1-58.

Shen W, Flajolet M, Greengard P, Surmeier DJ (2008) Dichotomous dopaminergic control of striatal synaptic plasticity. Science 321:848-851.

Smith Y, Wichmann T, Factor SA, DeLong MR (2012) Parkinson's disease therapeutics: new developments and challenges since the introduction of levodopa. Neuropsychopharmacology 37:213-246.

Squire LR (2004) Memory systems of the brain: a brief history and current perspective. Neurobiol Learn Mem 82:171-177.

Stuber GD, Hnasko TS, Britt JP, Edwards RH, Bonci A (2010) Dopaminergic terminals in the nucleus accumbens but not the dorsal striatum corelease glutamate. J Neurosci 30:8229-8233.

Sulzer D, Joyce MP, Lin L, Geldwert D, Haber SN, Hattori T, Rayport S (1998) Dopamine neurons make glutamatergic synapses in vitro. J Neurosci 18:4588-4602.

Swanson LW (1982) The projections of the ventral tegmental area and adjacent regions: a combined fluorescent retrograde tracer and immunofluorescence study in the rat.

Brain Res Bull 9:321-353.

Takashima I, Ichikawa M, Iijima T (1999) High-speed CCD imaging system for monitoring neural activity in vivo and in vitro, using a voltage-sensitive dye. J Neurosci Methods 91:147-159.

Taylor SR, Badurek S, Dileone RJ, Nashmi R, Minichiello L, Picciotto MR (2014) GABAergic and glutamatergic efferents of the mouse ventral tegmental area. J Comp Neurol 522:3308-3334.

Thabit MN, Nakatsuka M, Koganemaru S, Fawi G, Fukuyama H, Mima T (2011) Momentary reward induce changes in excitability of primary motor cortex. Clin Neurophysiol 122:1764-1770.

Thierry AM, Deniau JM, Herve D, Chevalier G (1980) Electrophysiological evidence for non-dopaminergic mesocortical and mesolimbic neurons in the rat. Brain Res 201:210-214.

Trojniar W, Staszewska M (1994) Unilateral damage to the ventral tegmental area facilitates feeding induced by stimulation of the contralateral ventral tegmental area. Brain Res 641:333-340.

Trudeau LE (2004) Glutamate co-transmission as an emerging concept in monoamine neuron function. J Psychiatr Neurosci 29:296-310.

Tseng KY, Mallet N, Toreson KL, Le Moine C, Gonon F, O'Donnell P (2006) Excitatory response of prefrontal cortical fast-spiking interneurons to ventral tegmental area stimulation in vivo. Synapse 59:412-417.

Ungerleider LG, Doyon J, Karni A (2002) Imaging brain plasticity during motor skill learning. Neurobiol Learn Mem 78:553-564.

von Kraus LM, Sacktor TC, Francis JT (2010) Erasing sensorimotor memories via PKMzeta inhibition. PLoS One 5:e11125.

Wang DV, Tsien JZ (2011) Conjunctive processing of locomotor signals by the ventral tegmental area neuronal population. PLoS One 6:e16528.

Watanabe Y, Kajiwara R, Takashima I (2009) Optical imaging of rat prefrontal neuronal activity evoked by stimulation of the ventral tegmental area. Neuroreport 20:875-880.

Williams SM, Goldman-Rakic PS (1998) Widespread origin of the primate mesofrontal dopamine system. Cereb Cortex 8:321-345.

Wise RA (2004) Dopamine, learning and motivation. Nat Rev Neurosci 5:483-494.

Xu T, Yu X, Perlik AJ, Tobin WF, Zweig JA, Tennant K, Jones T, Zuo Y (2009) Rapid formation and selective stabilization of synapses for enduring motor memories. Nature 462:915-919.

Yagishita S, Hayashi-Takagi A, Ellis-Davies GC, Urakubo H, Ishii S, Kasai H (2014) A critical time window for dopamine actions on the structural plasticity of dendritic spines. Science 345:1616-1620.

Yamaguchi T, Wang HL, Li X, Ng TH, Morales M (2011) Mesocorticolimbic glutamatergic pathway. J Neurosci 31:8476-8490.

Figure Legends

Figure 1.

Cortical dopamine (DA) nerve terminals in the primary motor cortex (M1) of rat. (A) Schematic drawing of a coronal section of rat forebrain at the level of the M1. Colored areas (orange) indicate cortical DA terminal fields; denser color indicates stronger DA innervation. (B) Schematic view of the two types of DA terminal. Cortical DA nerve terminals form both synaptic terminals (top) and non-synaptic terminals (Bottom). Colored circles (orange) indicate neurotransmitter DA. These figures were made according to Descarries et al. (1987, 2008). AI, agranular insular cortex; Cg, cingulate cortex; CPu, caudate putamen; M2, secondary motor cortex; NAcC/Sh, nucleus accumbens core/shell.

Figure 2.

The location of the ventral tegmental area (VTA) and substantia nigra pars compacta (SNc). (A) Schematic view of a sagittal section of the rat brain. The VTA (yellow) and SNc (light blue) located in ventral midbrain are source of cortical DA input. Number indicates the distance from midline (mm). (B) Schematic view of the midbrain coronal sections. Numbers indicate the distance from bregma (mm).

Figure 3. Principles of *in vivo* optical imaging with using VSD RH-795. (A) (Left) Exposed cortex is stained by filling the dental acrylic chamber with VSD RH-795 dissolved in ACSF (Red). The dye is infiltrated into the cortex during staining. (Right) The dye molecules are incorporated into extracellular side of the cell membranes, and emit fluorescence (red arrow) by irradiation of excitation light (green arrow). The signal from dye mainly originates from dendrite. (B) (Left) The intensity of the fluorescence from the dye decreased when membrane potential is depolarized by, for example, excitatory post synaptic potentials and action potentials. (Right) Fluorescence intensity is increased when the membrane potentials is hyperpolarized. Thus, the VSD convert the membrane potential fluctuation into the changes of fluorescence intensity.

Figure 4. The block diagram of the experimental system for performing the *in vivo* VSD imaging. Irradiation of the excitation from tungsten-halogen lamp to the exposed cortical surface was controlled by electromagnetic shutter. Excitation was projected through the band pass filter, and then dichroic mirror reflected it dawn onto the brain surface (green arrow). Optical devices were positioned on the target cortex. Fluorescence signal from the cortex is projected to the CCD image sensor through the dichroic mirror and long pass filter (red arrow). Optical characteristics of the filters and mirror are shown

in Appendix. Black solid lines indicate control signal, and dotted lines show the flow of acquired data. The triggers for VTA stimulation and data acquisition were controlled by micam01 system connected with the personal computer (PC). Electrical stimulation was applied to the VTA through concentric bipolar electrode. When LFP was recorded simultaneously with the VSD imaging. Glass electrode filled with 0.5M NaCl was carefully positioned near the cortical surface.

Figure 5. Optical signal exceeding the background level is color-coded. (A) Examples of raw fluorescence signal recorded from the cortex, which represent population membrane potentials. Baseline activity is shown as grey (left panel). Cortical depolarization and hyperpolarization are reported as decreasing (middle) and increasing (right) of optical signal, respectively. (B) Color-coded optical response. Green to red represent depolarization while blue to purple represent hyperpolarization. Color-coded histograms (bottom) represent relative number of color-coded pixels in each panel. (C) Color-coded optical signal exceeding the back ground level was superimposed on the bright-field image of the cortex. In this procedure, optical signal intensity close to the background level were ignored (White area in color-coded histograms and color bar). A, anterior; L, lateral.

Figure 6. VSD imaging of the motor cortical response after electrical stimulation of the VTA. (A) Schematic view of the experiment. The imaged cortical area, as indicated by a red rectangle, covered the motor cortex ipsilateral to the stimulated side. The borders between M1 and adjacent areas were delineated according to the brain atlas. (B) A spatiotemporal pattern of neuronal activity resulted from VTA stimulation. Single-pulse stimulation was applied at 0 ms, and the post-stimulus time is shown in each image. (C) The typical time course of optical signal (upper trace) and LFP (lower trace) recorded simultaneously from the M1. A triangle marks the stimulus onset. Fluorescence decrease is upward; upward or downward deflections of the signal indicate depolarization or hyperpolarization, respectively. The right traces are magnified view of the shaded areas in the left traces. Scale bar, 1.0 mm in (B).

Figure 7. Effect of stimulus intensity on VTA-evoked neuronal activity in M1. (A) Cortical activation pattern and optical signal traces evoked by VTA stimulation with different stimulus intensities. Optical signal traces were selected from the rectangle area in right panel. Arrows indicate the time points that are presented in the left panels. A triangle marks the stimulus onset. (B-C) The relationship between stimulus intensity and M1 responses were assessed by the peak amplitude and the half-width duration of the

optical signals (average of five trials from one rat). The excitatory or inhibitory components of the optical signal are indicated in red or blue, respectively. (B) The peak amplitude of the excitatory signal significantly increased with higher stimulus current. (C) The inhibitory signal was gradually prolonged when a stronger stimulus current was applied. Data are means ± SEM; *, $p < 0.05$; **, $p < 0.01$. Scale bar, 1.0 mm in (A).

Figure 8. The location of the stimulation sites. (A) An example of Nissl-stained midbrain section. Electrolytic lesion was made at the stimulation site (red dotted circle). Stimulation site was identified referring to the anatomical landmarks. (B) Stimulus sites either evoked (red circles, n=20) or fail to evoked (blue crosses, n=4) an M1 response. Each symbol indicates one animal. Numbers indicate the distance from bregma. R, red nucleus; IF, interfascicular nucleus, IP, interpeduncular nucleus; fr, fasciculus retroflexus; ml, medial lamniscus. Scale bar, 500 μm in (A).

Figure 9. VSD imaging of the motor cortical response after electrical stimulation of the VTA/SNc. (A) Example of TH-stained section with three electrolytic marker lesions (a-c), which are located within the VTA (a), SNc (b-c). TH immunopositive DA neurons and fibers were stained as black by nickel-DAB. (B) A spatiotemporal pattern of neuronal

activity resulted from VTA/SNc stimulation. Activation pattern in each rows (a-c) correspond to stimulation sites described in (A), respectively. Similar activation pattern were observed between VTA stimulation (a) and SNc (b-c) stimulation. (C) Optical signal traces selected from the small rectangle described in right panel. TH, tyrosine hydroxylase. Scale bar, 500 μm in (A), and 1.0 mm in (B).

Figure 10. VTA-evoked neuronal activity spreads from the CFA to the RFA in the motor cortex. (A) Initial activation sites and the direction of neuronal propagation. Filled circles indicate the site of initial activation in each animal, and the tip of the arrow indicates the center of gravity of the activity map 6 ms after the initial activation. (B) Motor representations in the M1 as plotted on a single frame of VTA-evoked neuronal activity. ICMS mapping was conducted immediately after VSD imaging. Colored circles indicate electrode penetration sites and the body parts moved by stimulation. (C) Three regions of interest (ROIs) selected in the motor cortex: CFA, RFA and Vib. The position of each ROI was determined by consulting the motor maps from three rats. The red and blue contour lines delineate CFA and RFA representations, respectively. (D–E) Peak amplitude and latency of VTA-evoked optical signals in three ROIs. (D) The peak amplitudes of the optical signals in both forelimb areas (CFA, RFA) were greater than that in the Vib. To

quantify the response amplitude without variation among animals, ΔF/F was normalized to the maximum response value of each animal, $(\Delta F/F)_{norm}$. (E) The latency-to-peak of the excitatory optical signal was significantly shorter in the CFA as compared with the RFA and the Vib. **, $p < 0.01$. CFA, caudal forelimb area; RFA, rostral forelimb area; Vib, vibrissae motor area. Scale bar, 1.0 mm in (B).

Figure 11. Motor cortical response after electrical stimulation of the CFA. (A) A spatiotemporal pattern of neuronal activity resulted from the CFA stimulation at different stimulus depths. Single-pulse stimulation was applied at the 500, 1000 and 1500 μm from cortical surface through the glass electrode. (B) Time contour maps indicate the extent of cortical areas where signal intensity larger than half maximum at that trial. (C) Motor representations was examined after the VSD imaging. Each colored circle indicate the motor representation at that stimulation site (D) Optical signal traces selected from the RFA (a) and the CFA (b), which depicted as small rectangles in the right panel. Triangle marks stimulus onset. (E) The time difference between the optical signal in the RFA and CFA (average of four trials from one rat). Peak latency of the RFA was subtracted by that of the CFA. *, $p < 0.05$.

Figure 12. VSD imaging of VTA-evoked neuronal activity in the M1 before and after application of CNQX, bicuculline, or a D1/D2 receptor antagonist to the cortical surface. (A) Neuronal activity completely disappeared after CNQX application. Upper right panels show the recovered response after CNQX washout. (B) Bicuculline completely eliminated inhibitory neuronal activity and greatly enhanced the excitatory response. (C) The D1 receptor antagonist SCH 23390 and the D2 receptor antagonist sulpiride had no effect. VSD imaging was performed 1 h after the administration of dopamine antagonists. Traces to the right of the images show the time course of the recorded optical signals. Scale bar, 1.0 mm.

Figure 13. Distribution of TH-positive fibers in the M1 of control rats. (A) Photomicrograph of a TH-stained M1 section. (B–D) Higher magnification of the regions shown in (A). TH-positive fibers were rich in layer 6, and sparsely distributed in the other cortical layers. Scale bar, 100 μm.

Figure 14. Stimulation of 6-OHDA-treated VTA fails to evoke neuronal activity in M1. (A) Schematic view of the experimental design. Electrical stimulation was applied to the 6-OHDA-treated VTA or the forelimb of the VTA-intact side. (B) Micrograph of a TH-

stained section including VTA. An arrow in the 6-OHDA-administered VTA indicates the electrolytic lesion made at the stimulation site. (C) Fluorescence image of a TH-stained section of M1 obtained from a 6-OHDA-lesioned rat (top). Cortical layers were delineated using Nissl staining of the same section (bottom). (D) VSD imaging of neuronal activity after the stimulation of the VTA (upper panels) or forelimb (lower panels). Representative optical signals that selected from the M1 and S1 are shown on the right. No response was observed following stimulation of the 6-OHDA-treated VTA, while the forelimb stimulation activated the sensorimotor cortex, including the M1 and S1. The latter result indicates that diminished M1 activity in the case of VTA stimulation was not caused by damage to the imaging cortex. S1, primary somatosensory cortex. 6-OHDA, 6-hydroxydopamine. Scale bar, 500 μm in (B), and 1.0 mm in (C) and (D).

Figure 15. Unilateral VTA stimulation elicits activation in the bilateral M1. (A) Schematic view of the experimental design. After unilateral VTA stimulation, VSD imaging was performed in the bilateral M1. Red rectangles indicate the imaged cortical areas. Muscimol was injected into the M1 ipsilateral to the stimulated VTA. (B–E) VTA-evoked responses in the ipsilateral and contralateral M1 before muscimol injection. (B) In the control, electrical stimulation of unilateral VTA elicited excitatory-inhibitory

neuronal activities in the bilateral M1. (C) The initial activation sites and the direction of neuronal propagation in the contralateral M1. The distribution pattern was similar to that in the ipsilateral M1, as shown in Fig. 10A. (D) Magnified and smoothed traces of the rising phase of the optical signals. The traces are from selected pixels in the area of initial activation. ΔF/F was normalized to the maximum response amplitude of each hemisphere. The contralateral response (blue) was significantly delayed compared with the ipsilateral response (black). (E) The VTA-evoked response amplitude was compared between hemispheres. The optical signals were collected from the CFA of the M1, and their peak amplitude was evaluated as the value of $\Delta F/F_{norm}$. The contralateral M1 showed reduced activation compared with the ipsilateral, but the difference was not significant ($p > 0.05$, Mann-Whitney U test). (F) VTA-evoked responses after muscimol injection. Neuronal activity in the muscimol-injected M1 (ipsilateral to the stimulated VTA) was completely abolished; however, the activity in the contralateral M1 was mostly unaffected. Arrows (pink) indicate muscimol injection sites. Traces on the right show representative optical signals obtained from the bilateral M1 before (black) and after (red) muscimol injection. Scale bar, 1.0 mm in (B) and (F).

Figure 16. Corpus callosum (CC) transection abolishes the contralateral M1 response.

(A) Schematic illustration of CC transection. A wire knife with a cannula was inserted through a cranial hole drilled above the olfactory bulbs (OBs). (B) Nissl-stained coronal section showing that the dorsal part of CC was cut without massive damage to the nearby cortex or underlying brain tissues. Complete transection of CC was not necessary in this experiment. Arrowheads indicate the borders between the M1 and surrounding cortical areas. (C–D) Spatiotemporal dynamics of VTA-evoked responses in the bilateral M1 before and after CC transection. (C) Stimulation of the right VTA (Rt-VTA) activated both the right M1 (Rt-M1, upper panels) and the left M1 (Lt-M1, lower panels) before CC scission. (D) After CC section, right VTA (Rt-VTA) stimulation activated the right M1 (Rt-M1, top panels) as usual, but the neuronal response disappeared in the left M1 (Lt-M1, middle panels). Under this condition, the left M1 (Lt-M1) exhibited typical ipsilateral neuronal activity in response to left VTA (Lt-VTA) stimulation (bottom panels). OB, olfactory bulb; CC, corpus callosum; M2, secondary motor cortex; Rt/Lt; right/left. Scale bar, 1.0 mm in (B), (C) and (D).

Figure 17. Current source density (CSD) analysis in the bilateral M1. (A) Photograph of the 16-channel electrode (left) and an example of a Nissl-stained section showing the needle track and the location of electrode contacts (right). (B–C) Depth profiles of LFPs

in response to VTA stimulation and corresponding CSD analyses in the ipsilateral and contralateral M1, respectively. In the CSD analyses, the size and the location of current sinks (reddish) and sources (bluish) are color-coded. The white triangle indicates stimulus onset.

Figure 18. The contralateral M1 response also arises from VTA-DA neurons. (A) Schematic view of the experimental design. Unilateral 6-OHDA animals were used. Electrical stimulation was applied to 6-OHDA-treated VTA (right) or intact VTA (left). VSD imaging was performed in the left M1 (VTA-intact side). (B) Photomicrograph of a TH-stained section including electrolytic lesions at the stimulation sites (arrows in bilateral VTAs). (C) Stimulation of the 6-OHDA-treated VTA failed to activate the contralateral M1 (upper panels), although the cortex exhibited normal excitatory-inhibitory neuronal activity when the intact VTA was stimulated ipsilaterally (lower panels). Traces under the images are the time courses of the optical signals. Scale bar, 500 μm and 1.0 mm in (B) and (C), respectively.

Figure 19. The ICMS-evoked electromyogram (EMG) response is modulated depending on the timing of conditioning VTA stimulation. (A) Schematic view of the

experimental design. (B–C) EMG of upper limb muscles in response to either VTA or M1 stimulation. Essentially no EMG response was observed after single pulse stimulation to the VTA (B). Here the intensity of M1 stimulation was below the movement threshold (C). (D) VTA stimulation preceded the ICMS by 10 ms. (E–F) the ICMS-evoked EMG was abolished when paired with the 30-ms preceding VTA-stimulation. The M1 stimulation with supra-threshold intensity evoked the EMG (E), but the muscle activity was precluded by the preceding VTA stimulation (F). (G–I) The EMG response started to reappear when the inter-stimulus interval was set to 40 ms (G). As the interval increased, the EMG response recovered gradually, and was restored by 200 ms (H, I). Gray lines indicate the EMG traces in each trial, and a red line indicates the mean EMG activity. Black triangles mark the stimulus onset. (J) A possible explanation for the time-dependent suppression of EMG. Traces show the time course of the VTA-evoked optical signal and its time derivative (red). The magnified inset on the right shows the initial phase. Differential operations were applied to the smoothened optical signal. The period during which the time derivative signal showed a large negative value (30–50 ms post-stimulation, shaded in gray) coincided with the period of strong EMG suppression (F, G).

Figure 20. Optical imaging of M1 activity in response to paired stimulation of VTA and

M1. (A) Layer 5 of M1 was stimulated by single electrical pulse using a glass electrode. (B) Time course of the optical signals recorded in the area “a” in (A). Red and black triangles indicate the onset of M1 and VTA stimulation, respectively. The upper two traces shows the control responses when M1 or VTA was stimulated alone. The other traces show the responses to VTA-M1 paired stimuli. Inter-stimulus intervals (ISI) are indicated in the figure. (E-J) VSD imaging of M1 activity corresponding to the stimulus conditions as shown in (B). The facilitated M1 response is indicated in (G) and (C). In the panel (C), pixels at which the signal amplitude exceeded a certain threshold were counted during a time window of 50 ms after the VTA stimulation (shaded in the inset). In the panel (D), number of pixels was counted, at which the M1-evoked signal amplitude exceeded a certain level. In this analysis, the baseline was set to the signal level just before the M1 stimulation. The M1-ICMS response was suppressed at the ISI of 30-50 ms, but recovered at the ISIs longer than 100 ms. Although a small ICMS-evoked M1 response can be seen at the bottom row frames in (I) and (J), VSD imaging cannot represent the recovered M1-ICMS response because it is buried in the preceding VTA-induced inhibition (see the bottom trace in B). Scale bar in (A) and (E), 1.0 mm.

Figures

Figure 1

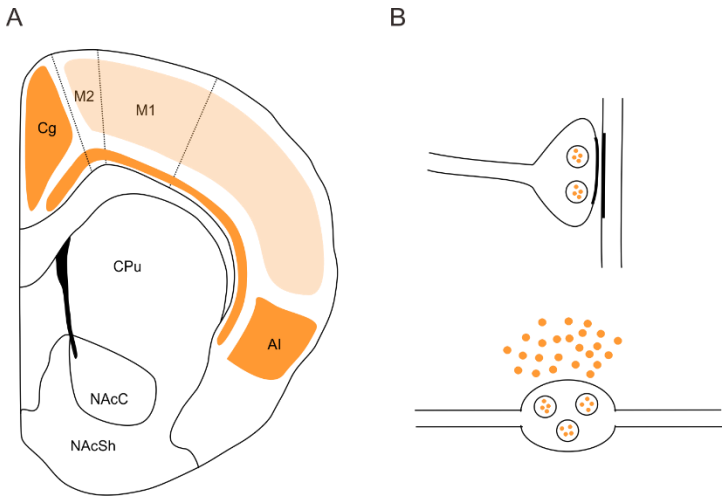

Figure 2

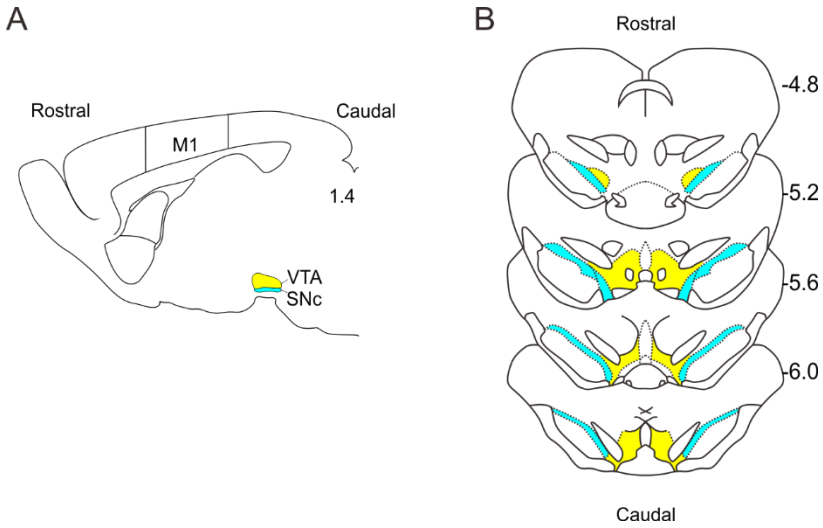

Figure 3

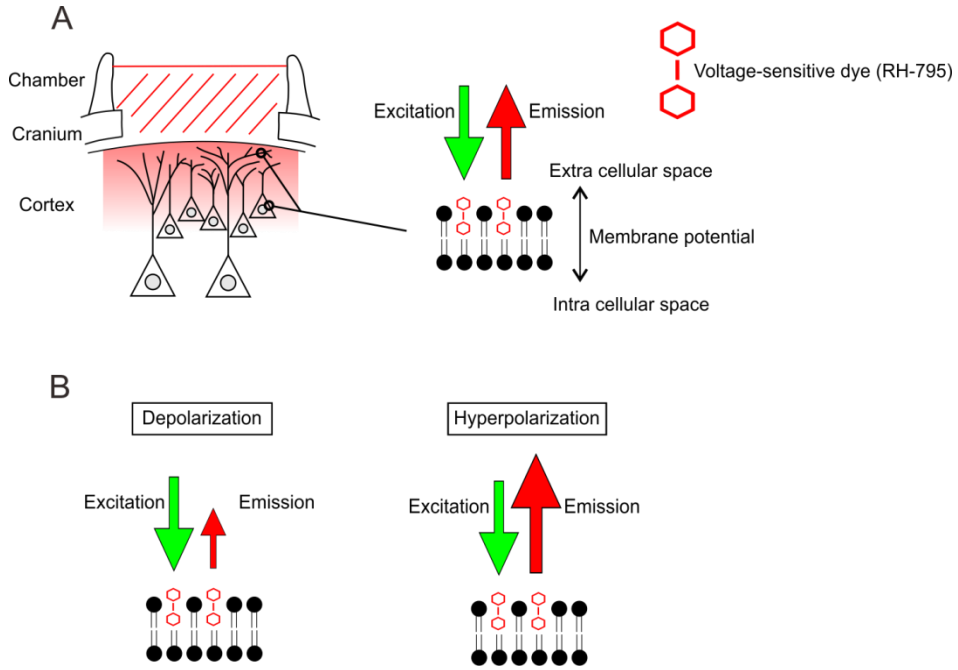
A
Chamber
Cranium
Cortex
Excitation
Emission
Voltage-sensitive dye (RH-795)
Extra cellular space
Membrane potential
Intra cellular space
B
Depolarization
Excitation
Emission
Hyperpolarization
Excitation
Emission

Figure 4

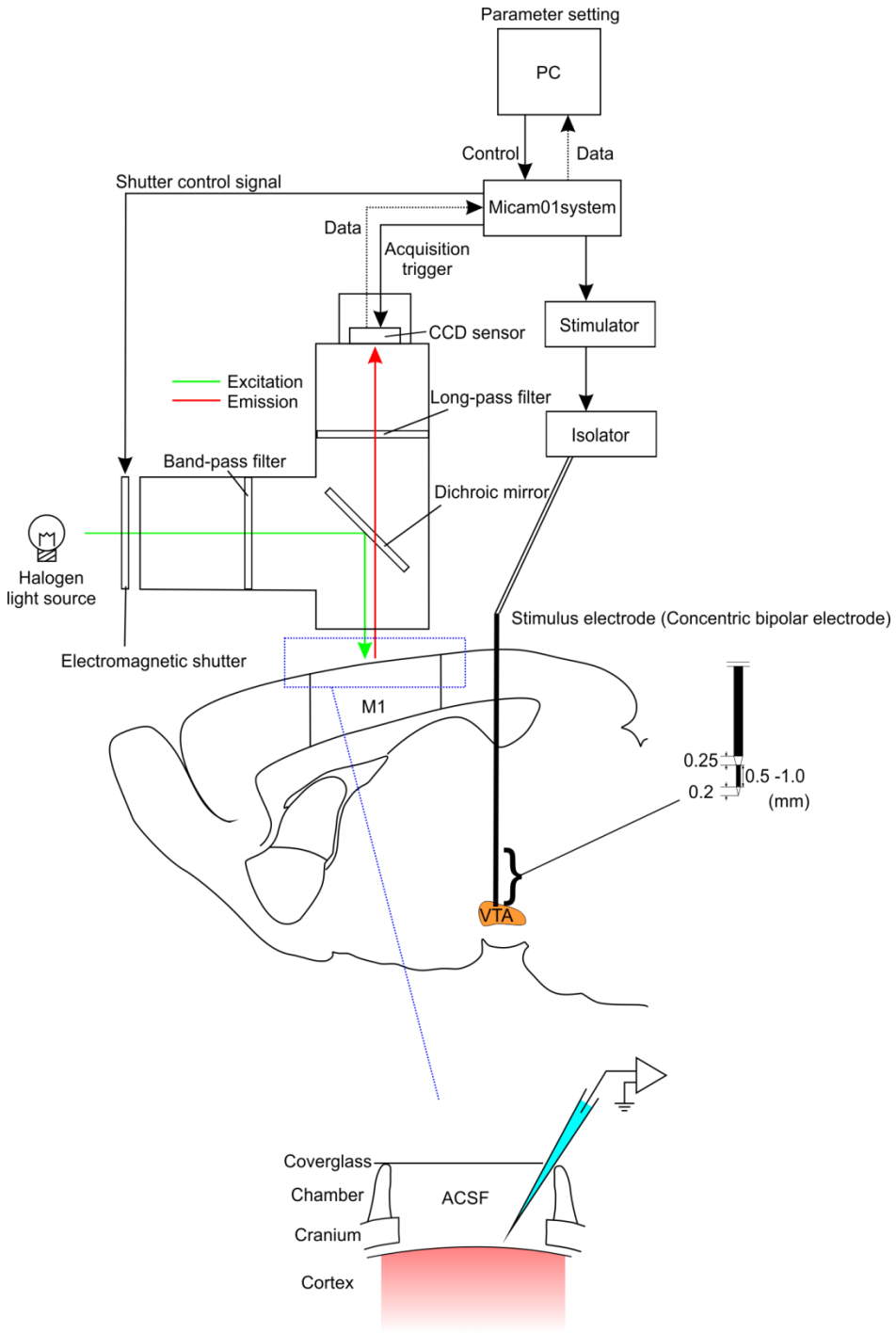
Parameter setting
PC
Control
Data
Shutter control signal
Micam01system
Data
Acquisition trigger
Stimulator
CCD sensor
Excitation
Emission
Long-pass filter
Isolator
Band-pass filter
Dichroic mirror
Halogen light source
Stimulus electrode (Concentric bipolar electrode)
Electromagnetic shutter
M1
0.25
0.2
0.5 -1.0 (mm)
VTA
Coverglass
Chamber
ACSF
Cranium
Cortex

Figure 5

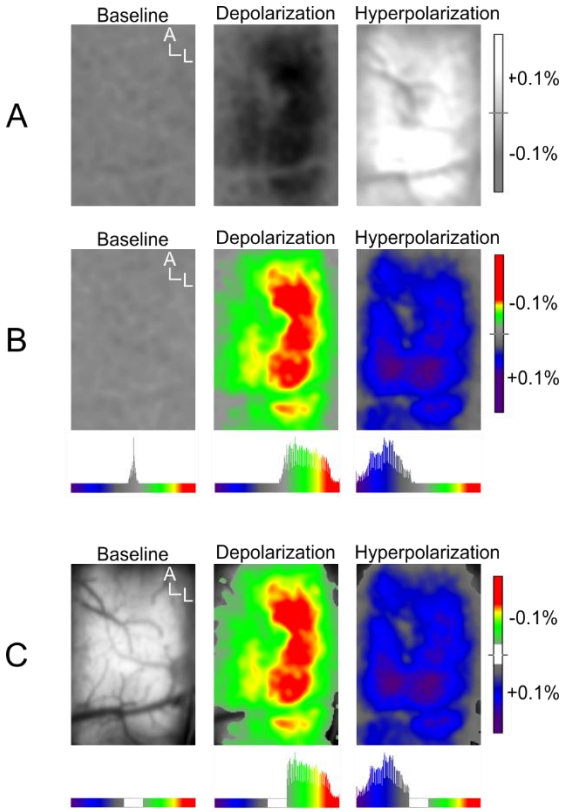
A
Baseline
Depolarization
Hyperpolarization
A
L
L
+0.1%
-0.1%
B
Baseline
Depolarization
Hyperpolarization
-0.1%
+0.1%
C
Baseline
Depolarization
Hyperpolarization
-0.1%
+0.1%

Figure 6

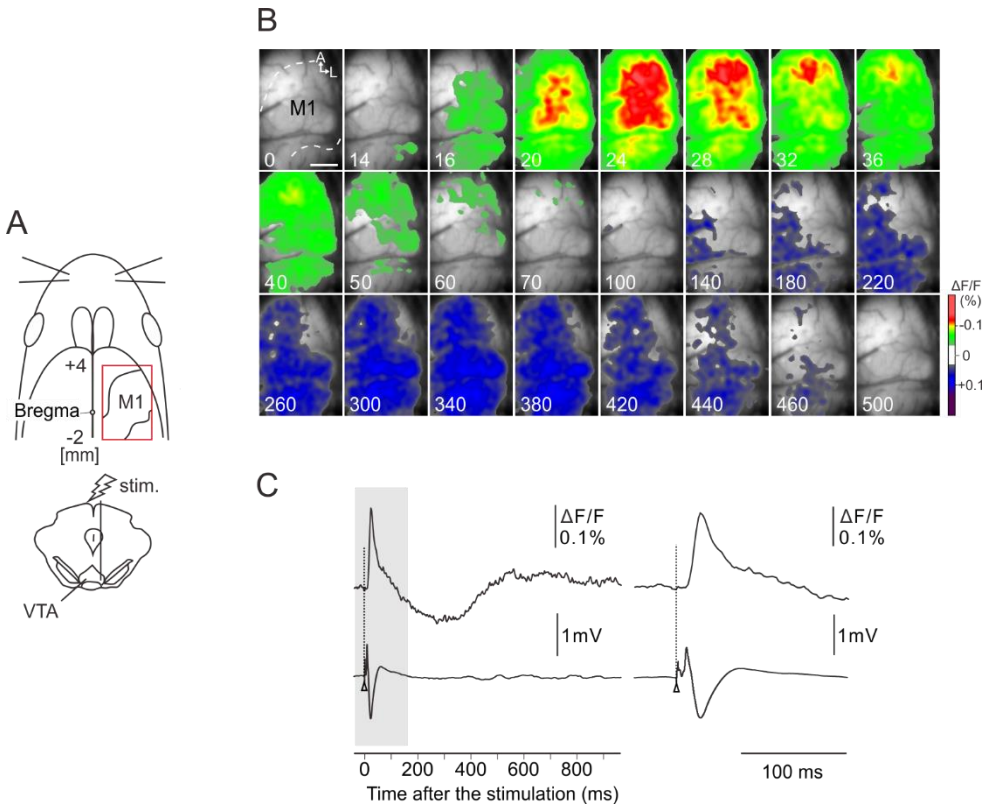
A
+4
Bregma
M1
-2
[mm]
stim.
VTA
B
M1
A
L
0
14
16
20
24
28
32
36
40
50
60
70
100
140
180
220
260
300
340
380
420
440
460
500
ΔF/F
(%)
0.1
0
+0.1
C
ΔF/F
0.1%
1mV
ΔF/F
0.1%
1mV
0
200
400
600
800
Time after the stimulation (ms)
100 ms

Figure 7

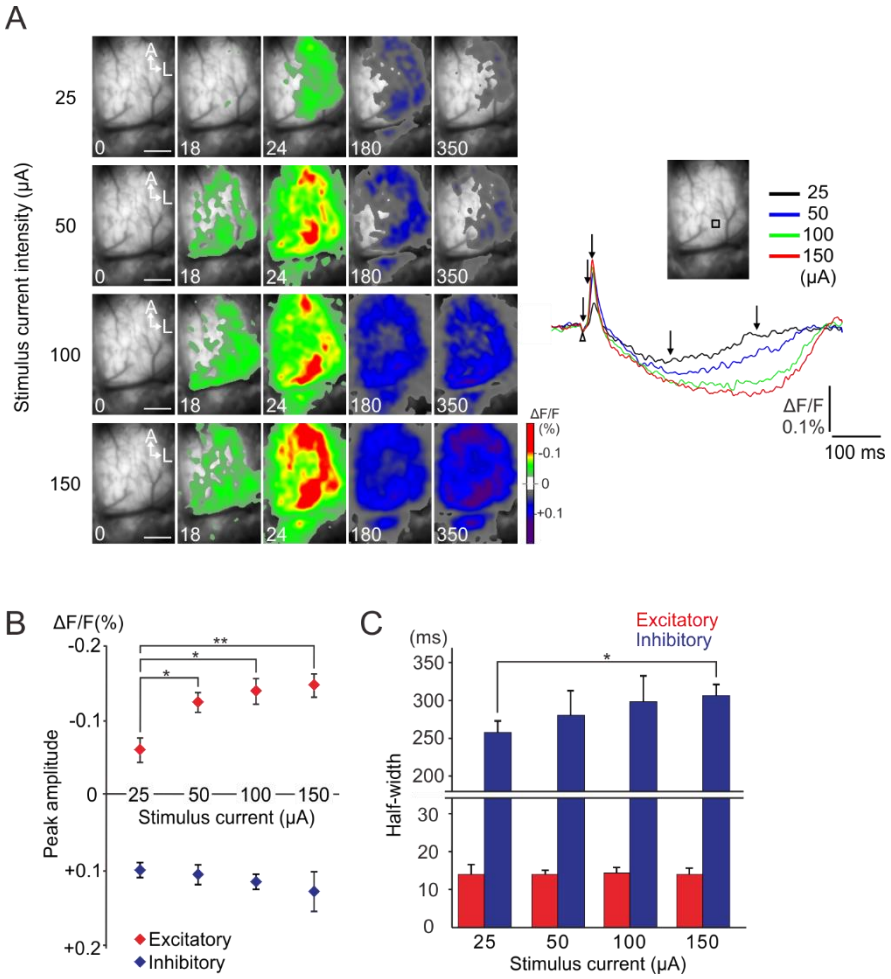
A
Stimulus current intensity (μA)
25
50
100
150
0
18
24
180
350
ΔF/F (%)
-0.1
0
+0.1
25
50
100
150
(μA)
ΔF/F
0.1%
100 ms
B
ΔF/F(%)
-0.2
-0.1
0
+0.1
+0.2
Peak amplitude
25
50
100
150
Stimulus current (μA)
Excitatory
Inhibitory
C
(ms)
Excitatory
Inhibitory
Half-width
350
300
250
200
30
20
10
0
25
50
100
150
Stimulus current (μA)

Figure 8

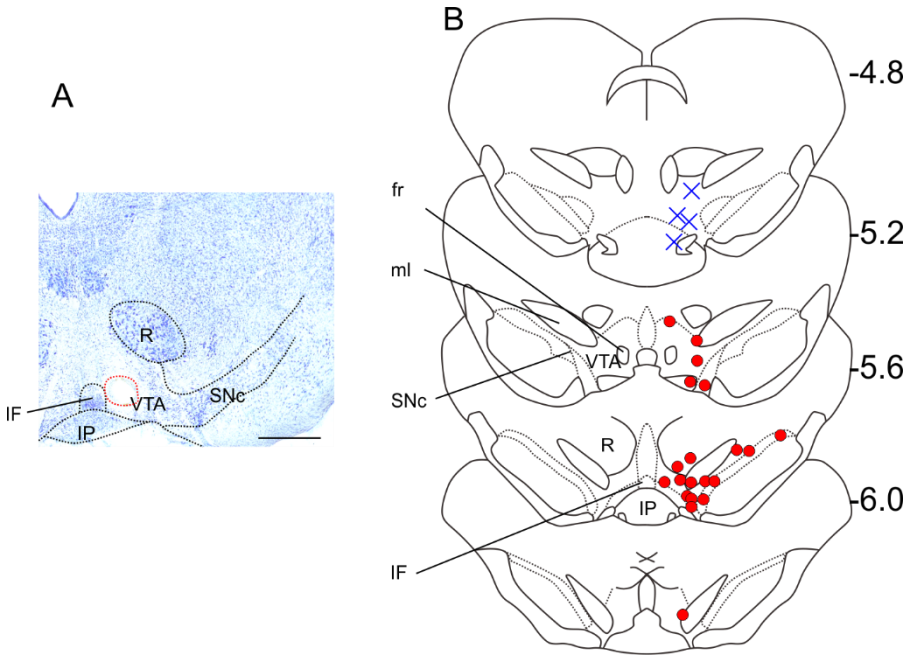

Figure 9

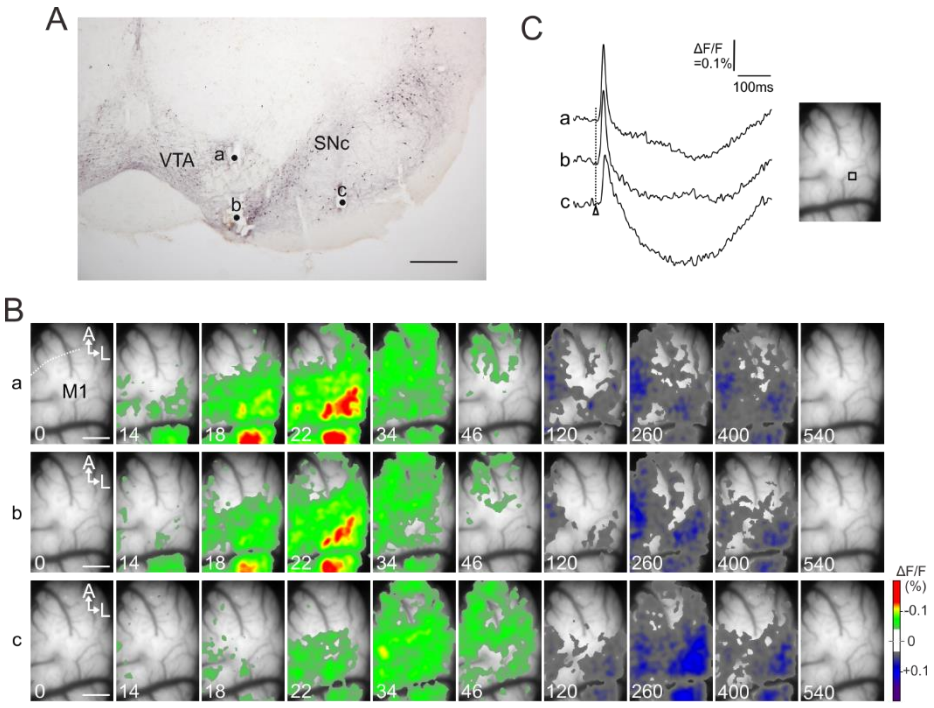
A
VTA
a
b
SNc
c
C
ΔF/F
=0.1%
100ms
a
b
c
B
M1
A
L
a
b
c
0
14
18
22
34
46
120
260
400
540
ΔF/F
(%)
-0.1
0
+0.1

Figure 10

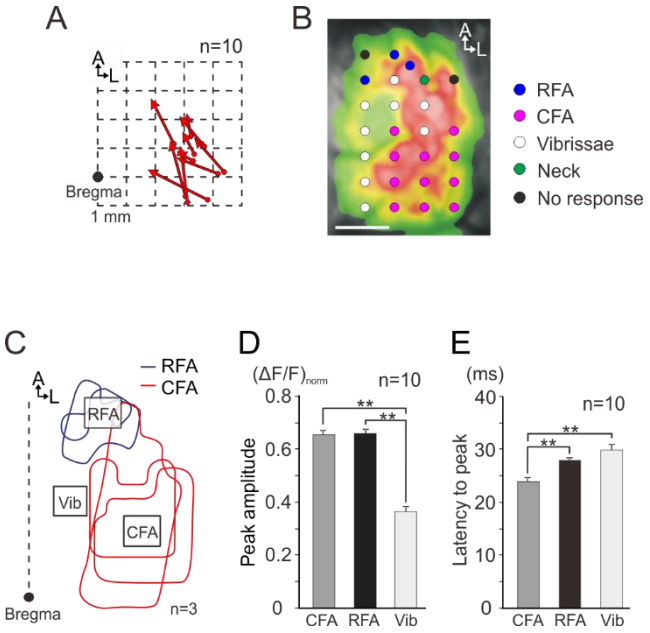
A
n=10
A
L
Bregma
1 mm
B
A
L
RFA
CFA
Vibrissae
Neck
No response
C
RFA
CFA
A
L
RFA
Vib
CFA
Bregma
n=3
D
(ΔF/F)norm
n=10
Peak amplitude
0.8
0.6
0.4
0.2
0
**
**
CFA
RFA
Vib
E
(ms)
n=10
Latency to peak
40
30
20
10
0
**
**
CFA
RFA
Vib

Figure 11

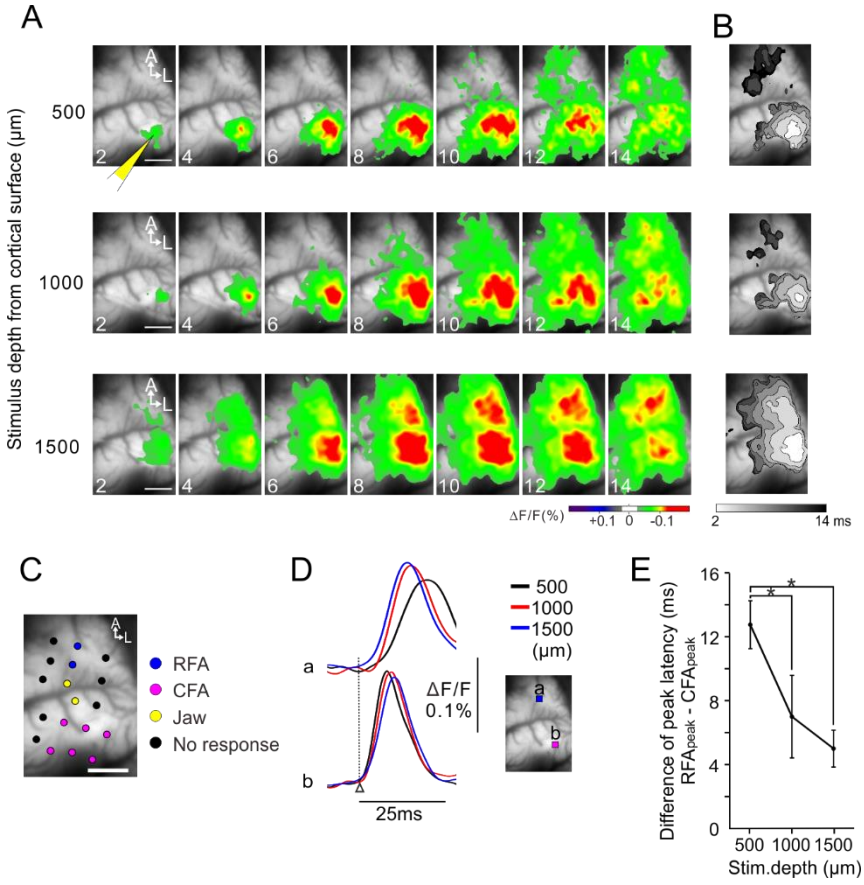
A
B
C
D
E
Stimulus depth from cortical surface (μm)
500
1000
1500
2
4
6
8
10
12
14
ΔF/F(%)
+0.1 0 -0.1
2
14 ms
RFA
CFA
Jaw
No response
a
b
ΔF/F
0.1%
25ms
500
1000
1500
(μm)
Difference of peak latency (ms)
RFApeak - CFApeak
Stim.depth (μm)

Figure 12

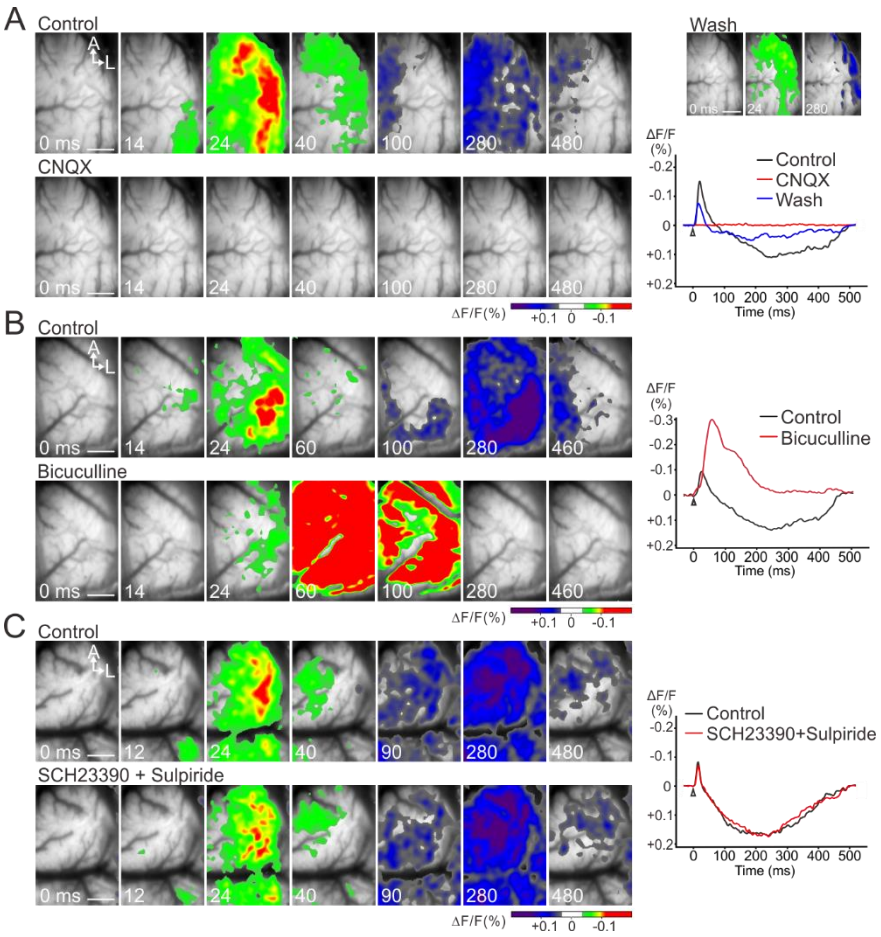
A
Control
A
L
0 ms
14
24
40
100
280
480
CNQX
Wash
ΔF/F(%)
+0.1 0 -0.1
ΔF/F (%)
Control
CNQX
Wash
Time (ms)
B
Control
60
460
Bicuculline
Bicuculline
C
12
90
SCH23390 + Sulpiride
SCH23390+Sulpiride

Figure 13

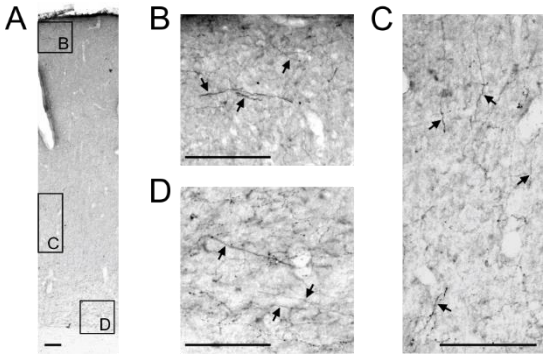

Figure 14

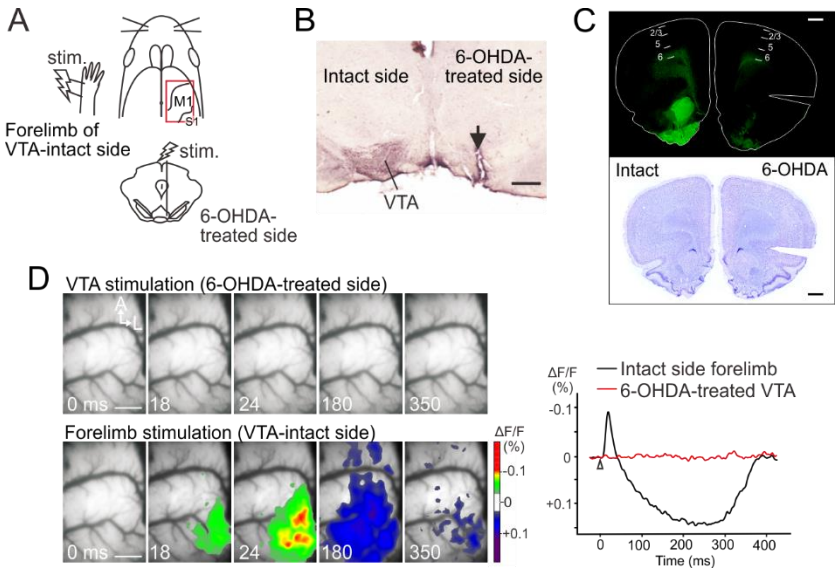
A
stim.
M1
S1
Forelimb of
VTA-intact side
stim.
6-OHDA-
treated side
B
Intact side
6-OHDA-
treated side
VTA
C
Intact
6-OHDA
D
VTA stimulation (6-OHDA-treated side)
0 ms
18
24
180
350
Forelimb stimulation (VTA-intact side)
ΔF/F
(%)
-0.1
0
+0.1
Intact side forelimb
6-OHDA-treated VTA
-0.1
0
+0.1
0
100
200
300
400
Time (ms)

Figure 15

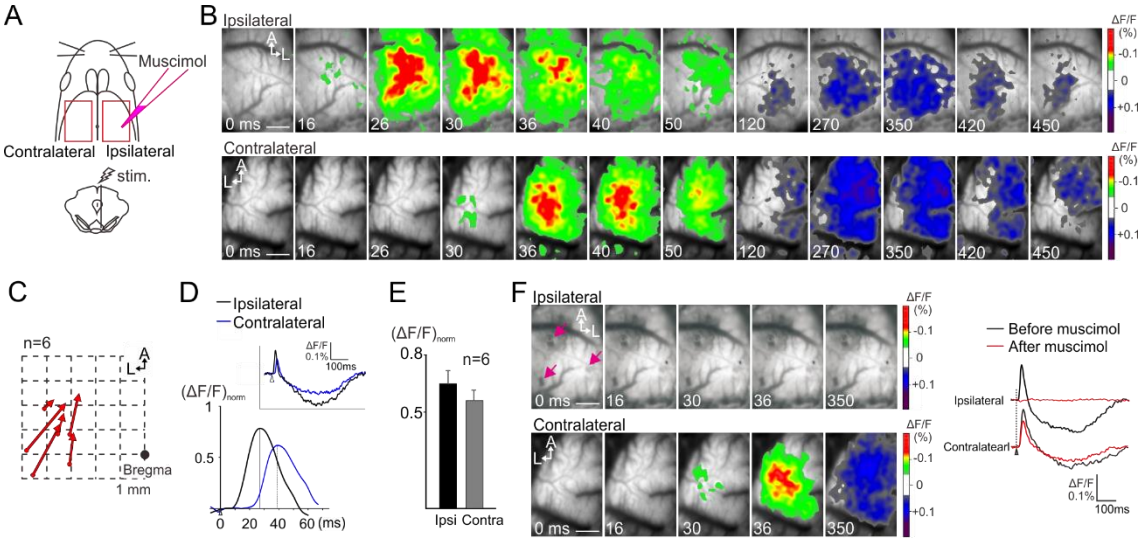
A
Muscimol
Contralateral
Ipsilateral
stim.
B
Ipsilateral
Contralateral
0 ms
16
26
30
36
40
50
120
270
350
420
450
ΔF/F
(%)
-0.1
0
+0.1
C
n=6
Bregma
1 mm
D
Ipsilateral
Contralateral
(ΔF/F)norm
ΔF/F
0.1%
100ms
0 20 40 60 (ms)
E
(ΔF/F)norm
n=6
Ipsi Contra
F
Ipsilateral
Contralateral
0 ms
16
30
36
350
Before muscimol
After muscimol
Ipsilateral
Contralateral
ΔF/F
0.1%
100ms

Figure 16

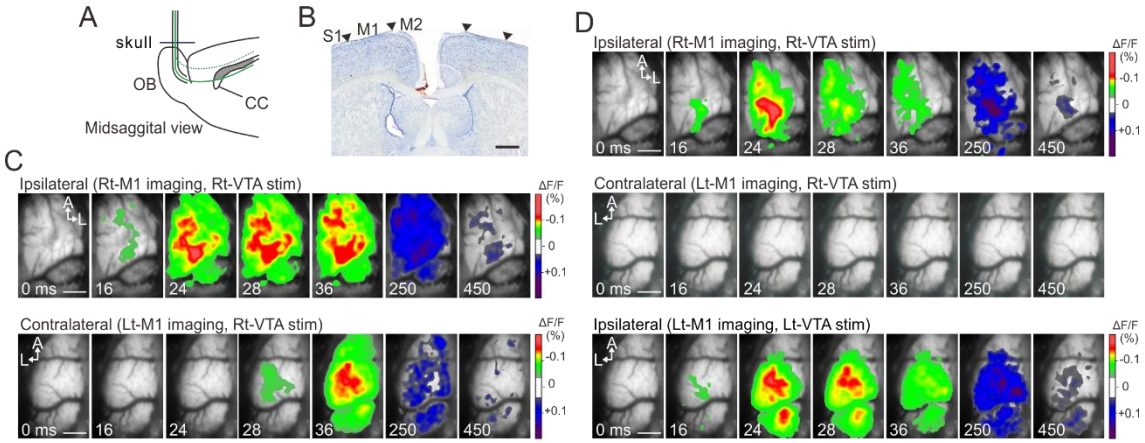
A
skull
OB
CC
Midsaggital view
B
S1
M1
M2
C
Ipsilateral (Rt-M1 imaging, Rt-VTA stim)
Contralateral (Lt-M1 imaging, Rt-VTA stim)
D
Ipsilateral (Rt-M1 imaging, Rt-VTA stim)
Contralateral (Lt-M1 imaging, Rt-VTA stim)
Ipsilateral (Lt-M1 imaging, Lt-VTA stim)
ΔF/F (%)
-0.1
0
+0.1
0 ms
16
24
28
36
250
450

Figure 17

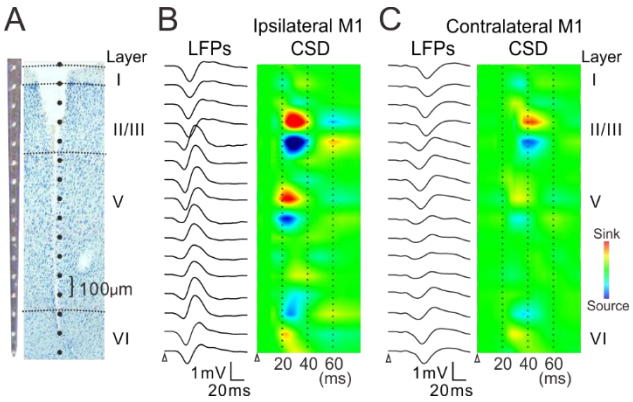
A
Layer
I
II/III
V
100μm
VI
B
Ipsilateral M1
LFPs
CSD
1mV
20ms
20 40 60
(ms)
C
Contralateral M1
LFPs
CSD
Layer
I
II/III
V
Sink
Source
VI
1mV
20ms
20 40 60
(ms)

Figure 18

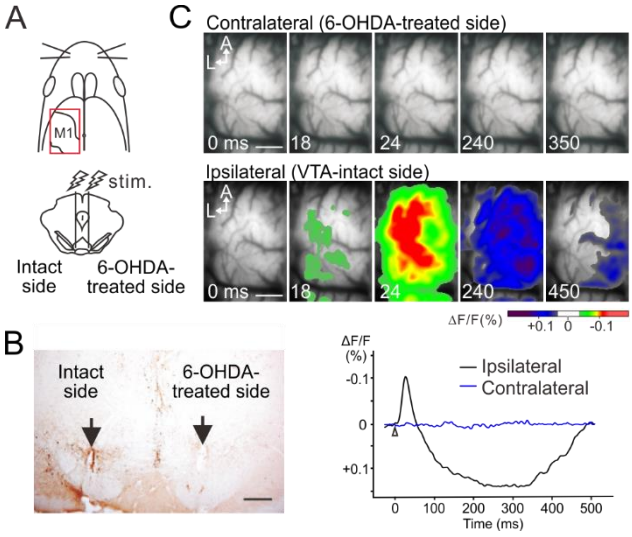
A
M1
stim.
Intact side
6-OHDA-treated side
B
Intact side
6-OHDA-treated side
C
Contralateral (6-OHDA-treated side)
A
L
0 ms
18
24
240
350
Ipsilateral (VTA-intact side)
A
L
0 ms
18
24
240
450
ΔF/F(%)
+0.1
0
-0.1
ΔF/F (%)
-0.1
0
+0.1
Ipsilateral
Contralateral
0
100
200
300
400
500
Time (ms)

Figure 19

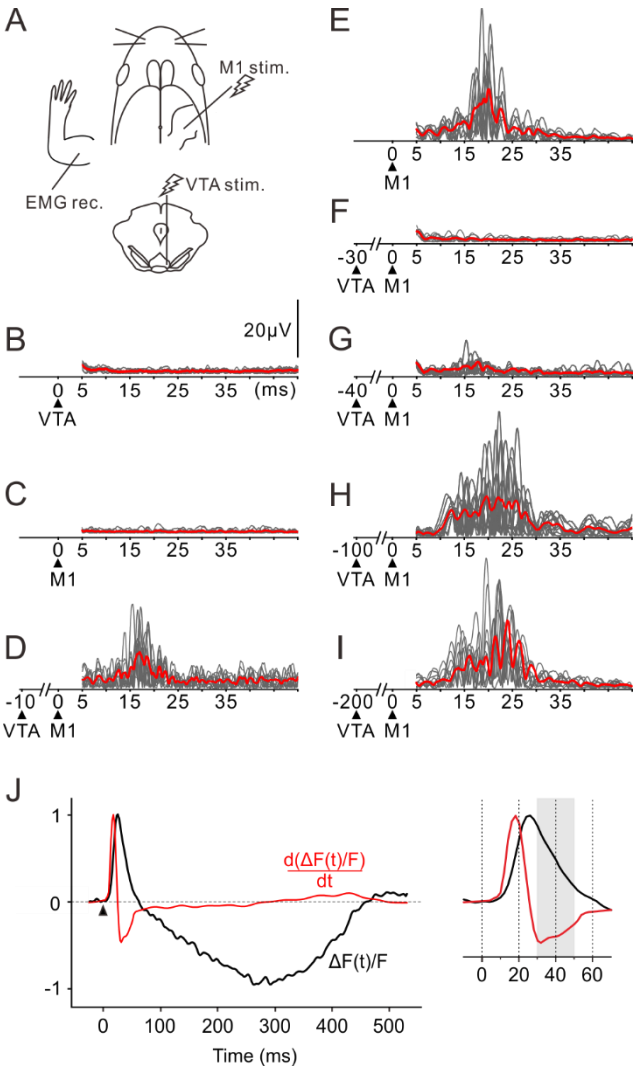
A
M1 stim.
EMG rec.
VTA stim.
B
20μV
0 5 15 25 35 (ms)
VTA
C
0 5 15 25 35
M1
D
-10 0 5 15 25 35
VTA M1
E
0 5 15 25 35
M1
F
-30 0 5 15 25 35
VTA M1
G
-40 0 5 15 25 35
VTA M1
H
-100 0 5 15 25 35
VTA M1
I
-200 0 5 15 25 35
VTA M1
J
1
0
-1
d(ΔF(t)/F)
dt
ΔF(t)/F
0 100 200 300 400 500
Time (ms)
0 20 40 60

Figure 20

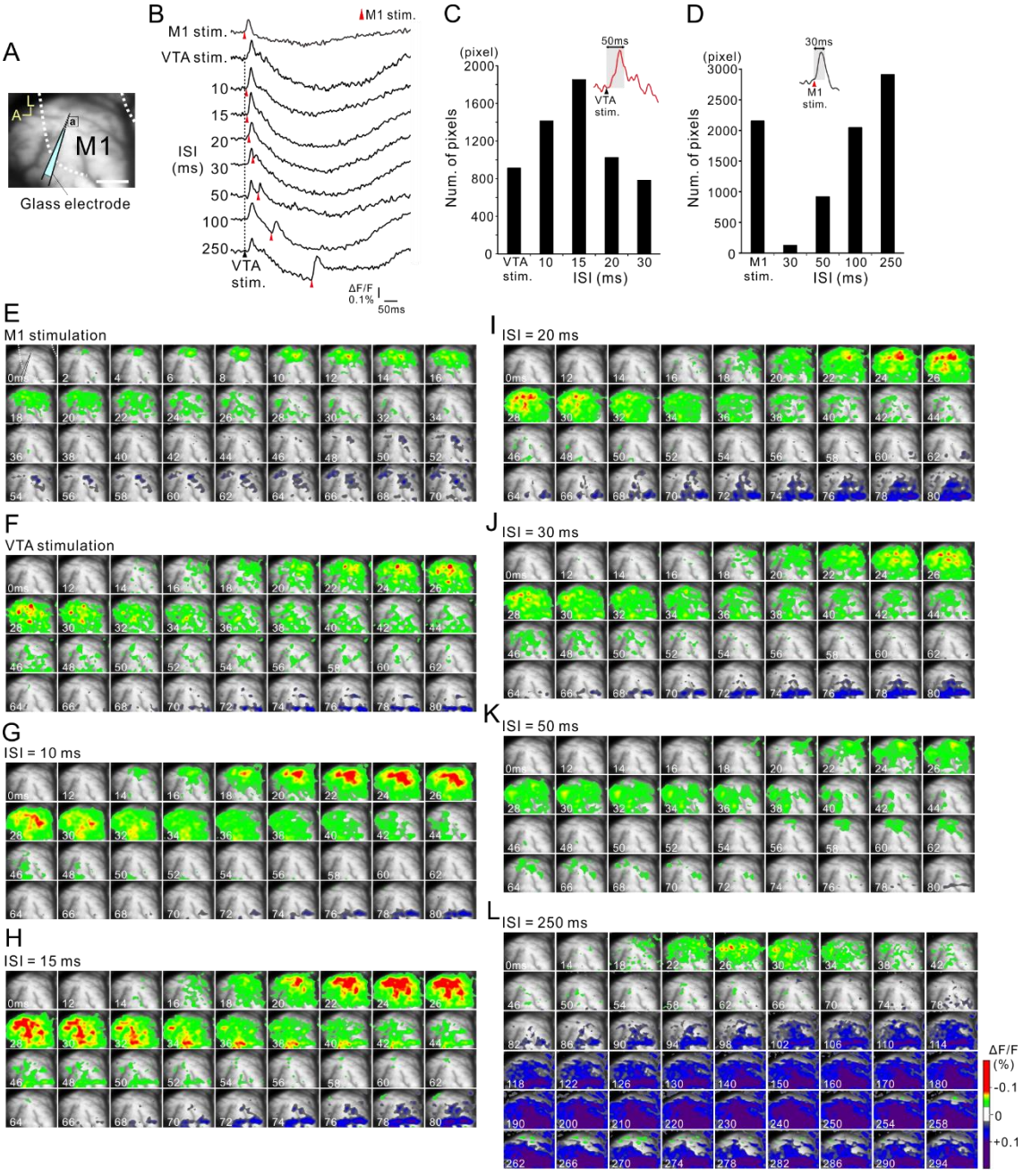
A
M1
Glass electrode
B
M1 stim.
VTA stim.
ISI (ms)
10
15
20
30
50
100
250
VTA stim.
ΔF/F 0.1%
50ms
C
(pixel)
Num. of pixels
50ms
VTA stim.
VTA stim. 10 15 20 30
ISI (ms)
D
(pixel)
Num. of pixels
30ms
M1 stim.
M1 stim. 30 50 100 250
ISI (ms)
E
M1 stimulation
F
VTA stimulation
G
ISI = 10 ms
H
ISI = 15 ms
I
ISI = 20 ms
J
ISI = 30 ms
K
ISI = 50 ms
L
ISI = 250 ms
ΔF/F (%)
-0.1
0
+0.1

Appendix

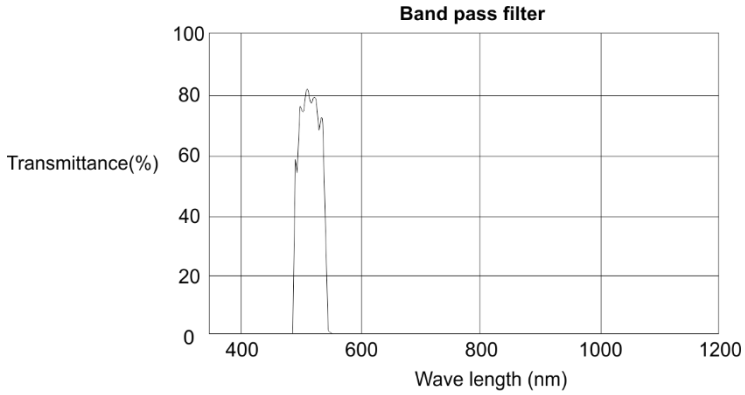
Band pass filter
Transmittance(%)
100
80
60
40
20
0
400
600
800
1000
1200
Wave length (nm)

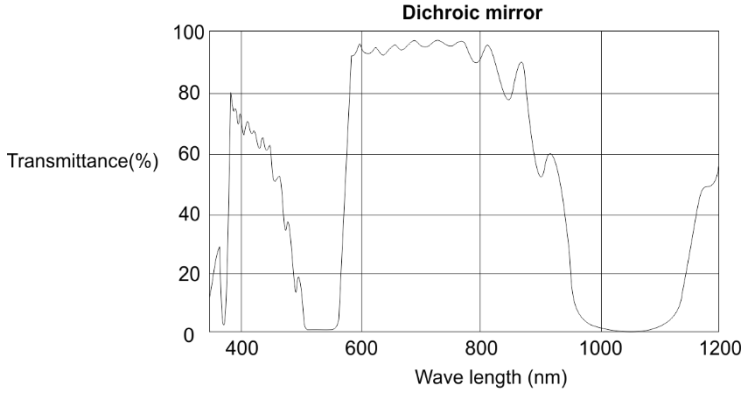
Dichroic mirror
Transmittance(%)
100
80
60
40
20
0
400
600
800
1000
1200
Wave length (nm)

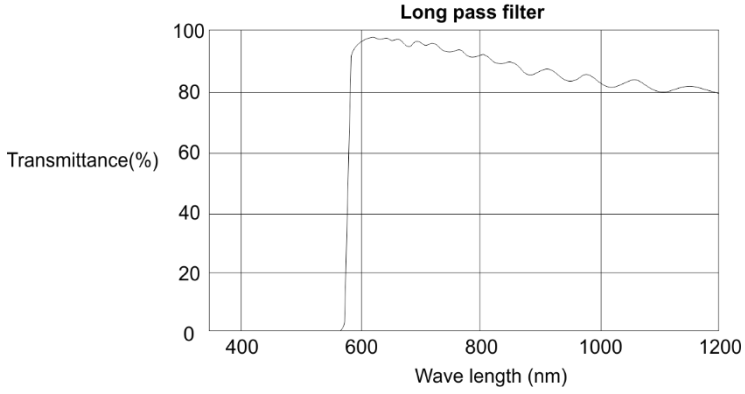
Long pass filter
Transmittance(%)
100
80
60
40
20
0
400
600
800
1000
1200
Wave length (nm)

Acknowledgements

I am deeply grateful to my supervisor Dr. Takashima for providing me this precious study opportunity as Ph. D student in his laboratory and warm encouragement during this study. I would also like to thank Dr. Kajiwara for valuable comments and discussion that helped me to successfully complete my research. Likewise, I want to thank Drs. Matsumoto, Ichitani, Mizuhiki, and Nishimaru for reviewing this article and administrative support during this study. I also thank to Drs. Higo, Watanabe, Shuto, and Hisano for histological verification and valuable comments.

Finally, I gratefully appreciate the support and encouragement of my family and friends.